University of Helsinki Report Series in Physics

HU-P-D249

Modelling of defect formation and evolution in metals and silicon

Laura Bukonte

Division of Materials Physics
Department of Physics
Faculty of Science
University of Helsinki
Helsinki, Finland

Academic Dissertation

To be presented, with the permission of the Faculty of Science of the University of Helsinki, for public criticism in auditorium XII of the Main Building of the University of Helsinki, on July 22 2017, at 12 o'clock noon.

Helsinki 2017

ISBN 978-951-51-2767-9 (printed version)
ISSN 0356-0961
Helsinki 2017
Unigrafia Oy

ISBN 978-951-51-2768-6 (PDF version)
http://ethesis.helsinki.fi/
Helsinki 2017
Electronic Publications @ University of Helsinki

Laura Bukonte, **Modelling of defect formation and evolution in metals and silicon**, University of Helsinki, 2017, 52 p. + appendices, Report Series in Physics HU-P-D237, ISSN 0356-0961, ISBN 978-951-51-2767-9 (printed version), ISBN 978-951-51-2768-6 (PDF version)

Abstract

Defects always exists in a crystal lattice at temperatures above absolute zero. Our knowledge of defect concentration and mobility is crucial, due to their profound influence on the material properties.

By the means of thermodynamics it is possible to estimate defect concentrations at the equilibrium conditions. Near the melting point of pure metals the vacancy fraction is typically about 10^{-4}. However, it has been shown that the presence of light impurities may enhance vacancy formation in many metals and metal alloys. The main reason for this phenomenon, often referred to as the superabundant vacancy formation, is the lowering of the vacancy formation energy due to the impurity trapping. In this thesis a theoretical thermodynamics model has been developed to study the equilibrium vacancy concentrations as a function of impurity concentration and temperature. Our model takes into account monovacancy and divacancy thermodynamics as well as the binding energy of each trapped impurity and the vibrational entropy of defects.

The diffusion of monovacancies and hydrogen in tungsten is studied due to its relevance to fusion research. Extraordinary thermal and mechanical properties, like high melting temperature, high heat conductivity, low sputtering yield and low hydrogen retention makes tungsten a prime candidate for a divertor plate material in the next step fusion device ITER. At this region of the fusion reactor, the material is exposed to the highest heat and particle fluxes producing damage in the plasma facing components. Open volume defects are known to trap hydrogen and, thus, are the main reasons for hydrogen retention in tungsten. The radioactive hydrogen isotope tritium retention in the fusion reactor is especially undesirable due to efficiency and safety reasons.

The molecular dynamics method has been used to simulate the diffusion of hydrogen in tungsten. The commonly accepted and so far used H diffusion migration barrier is revised and a new analysis method to determine diffusion coefficients that accounts for the random oscillation of atoms around the equilibrium position is presented. At high hydrogen concentrations, a dramatic reduction in the diffusion coefficient is observed, due to the neighbouring interstitial

site blocking and the repulsive interaction between the hydrogen atoms. The results of this study indicate that high flux hydrogen irradiation would lead to much higher H concentrations in tungsten than previously expected.

The diffusion through the vacancy mechanism is the dominating mechanism behind self-diffusion in most metals and substitutional alloys. However, the precise self-diffusion experimental measurements show that some FCC and BCC metals exhibit non-Arrhenius behaviour of self-diffusion close to the melting point. Several mechanisms have been proposed to interpret the slight upward curvature of the Arrhenius diagram. The results of this study obtained employing molecular dynamics method show the presence of multiple nearest neighbour jumps of monovacancy above 2/3 of the melting temperature of tungsten. For the first time, the W monovacancy diffusion prefactor is calculated, and found to be unexpectedly high, resulting in a monovacancy diffusion attempt frequency of about 2-3 orders of magnitude higher than the values commonly used.

A comparative study between the molecular dynamics and a Monte Carlo method – binary collision approximation has been carried out in this thesis by simulating the single ion impacts on silicon and tungsten surfaces. It has been experimentally shown that cumulative ion impacts can result in surface pattern formation. Under certain conditions, periodic patterns such as ripples may form. This phenomenon has been studied for decades and several theoretical models for ripple formation have been proposed. A recent theoretical model based on the displacement analysis from molecular dynamics simulations suggest that the main mechanism responsible for the ripple formation is atom redistribution upon the ion impact, sputtering being less important. Molecular dynamics is limited in the size of systems that it can model, creating a demand for computationally more efficient methods to study ion irradiation effects, such as binary collision approximation. The results from both methods are compared and found to be in a good agreement for crystalline structures. However, large discrepancies between the two methods arise for materials that are amorphous or become amorphized during ion irradiation. The binary collision approximation approach does not account for a very large number of small displacements seen in molecular dynamics that are attributed to the collective phenomenon of amorphous material flow. This shortcoming can seriously compromise the ability to use the binary collision approximation for explaining such phenomena as surface pattern formation, where small displacements play a central role.

Contents

Common Abbreviations

a-Si	Amorphous Silicon
BCA	Binary Collision Approximation
BCC	Body Centered Cubic
BOP	Bond Order Potential
c-Si	Crystalline Silicon
Co	Cobalt
EAM	Embedded Atom Model
EDIP	The Environment-Dependent Interatomic Potential
FCC	Face Centered Cubic
Fe	Iron
H	Hydrogen
IS	Interstitial Sites
MD	Molecular Dynamics
Ni	Nickel
OIS	Octahedral Interstitial Sites
PARCAS	PARallell CAScade
Pd	Palladium
SAV	Superabundant Vacancy
TIS	Tetrahedral Interstitial Sites
TS	Trapping Sites
Si	Silicon
W	Tungsten

Chapter 1

Introduction

'Crystals are like people: it is the defects in them which tend to make them interesting!' – Colin Humphreys.

In nature solids are rarely perfectly ordered. Above temperatures of 0 K, imperfections in a crystalline structure are always present. Imperfections in the materials are called defects and may be categorized by their size – zero, one, two and three dimensional defects. The zero dimensional defects include isolated vacancies and impurity atoms, and are commonly referred to as the point defects. Defects such as dislocations and crowdions are considered one-dimensional. Grain boundaries and external surfaces are thought of as the two-dimensional defects, and three-dimensional defects are volume imperfections in the crystal that include voids, precipitates or the presence of a different phase.

Another useful way to classify defects is to distinguish between intrinsic and extrinsic defects. Intrinsic defects are imperfections in a pure material, such as vacancies and self-interstitial atoms. Extrinsic defects, on the other hand, are caused by the presence of impurity atoms.

According to thermodynamics, nature always tries to minimize its free energy. In order to create a defect a certain amount of energy is needed. However, the presence of a defect in the lattice also increases the entropy of the system, reducing the free energy of the system. Defects will increase in their concentration until the free energy reaches its minimum - systems in this state are said to be in thermodynamic equilibrium.

Defects profoundly affect the physical, mechanical and electrical properties of materials and their presence in materials can be desired or unwanted.

In a fusion reactor, high heat and particle fluxes damage the plasma facing components, creating vacancies and other open volume defects that act as trapping centres for hydrogen (H) isotopes. It is especially undesirable due to the retention of the radioactive isotope of H - tritium.

The ion irradiation processes can be used to intentionally alter material properties. Introducing foreign impurities in pure semiconductor materials, changing the electron and hole concentrations, is called doping and is the basis in modern electronic device technology. Using ion beams, it is possible to modify the morphology of surfaces to form periodic structures such as ripples.

To predict the performance of materials, studying their structures and estimating defect production is essential. Defects can be studied employing various methods. A suitable method for calculating the equilibrium concentration of defects is the thermodynamics approach. The defect formation energies and migration barriers can be determined using the first principle methods. The dynamics of defects can be addressed employing molecular dynamics. The damage to materials upon the irradiation can be computationally most efficiently studied using binary collision approximation simulations. Many experimental methods exist to investigate defects in materials. Positron annihilation spectroscopy is commonly used to estimate vacancy concentration in crystals [1]. Secondary ion mass spectrometry provides the information on the composition of the material and the impurity depth profiles [2–4]. To estimate vacancy formation upon light impurity presence in a lattice, a temporal variation of a lattice parameter at high temperature and high H pressures can be measured by X-ray diffraction. Temporal electrical resistivity measurements as a function of temperature, pressure and H concentrations also have been used to estimate the vacancy formation influenced by impurities in various metals.

The present thesis is focused on studying the formation of vacancies in metals in the presence of H impurities by applying thermodynamic calculations. Due to its relevance to fusion research, the monovacancy and H diffusion in tungsten is studied using molecular dynamics simulations. A comparative study of two fundamentally different computational methods, molecular dynamics and binary collision approximation, is carried out to examine the atom displacements in silicon and tungsten upon ion irradiation.

Chapter 2

Purpose and Structure of this study

The purpose of this thesis is to provide a better understanding of defect formation and evolution in metals and silicon. The theoretical thermodynamics calculations are used to quantitatively estimate defect formation in metals. The molecular dynamics and binary collision approximation simulations are employed to study the diffusion of monovacancies and H impurities in tungsten and atom displacements upon ion irradiation in amorphous and crystalline silicon, and tungsten.

This thesis is based on four articles published in international peer-reviewed journals.

The structure of the thesis is as follows. In the following section, the four publications are summarized and the author's contributions are indicated. Chapter 3 contains the theoretical background on thermodynamics of defect formation and diffusion. Chapter 4 contains the theoretical background on the irradiation effects in solids. The methods used to study the defect dynamics are summarized in Chapter 5. In Chapter 6 the main results of the thesis are presented and discussed. The summary and main conclusions are provided in Chapter 7.

2.1 Summary of Original Publications

Publication I: Thermodynamics of impurity-enhanced vacancy formation in metals

L. Bukonte, T. Ahlgren and K. Heinola, *Journal of Applied Physics*, 121, 045102 (2017).

In this study, we develop a general theoretical thermodynamics model that allows us to study the thermodynamics of vacancy formation in metals with the presence of interstitial impurities. We study the vacancy formation as a function of temperature and the impurity concentration. For the correct description of free energy of the system, we take into account the binding energies of each trapped impurity, the vibrational entropy of defects and thermodynamics of divacancy formation. We show that vacancies are formed in metals due to the presence of H impurities, regardless of their binding energy to the vacancy. We demonstrate that the divacancy fraction gives a major contribution to the total vacancy fraction at high H fractions and cannot be neglected when studying superabundant vacancies. Our study leads to an important conclusion that SAV formation is more pronounced in the FCC phase compared to the BCC phase.

Publication II: Modelling of monovacancy diffusion in W over a wide temperature range

L. Bukonte, T. Ahlgren and K. Heinola, *Journal of Applied Physics* 115, 123504 (2014)

In this paper, we study the monovacancy diffusion in tungsten over a wide temperature range. Multiple nearest neighbour jumps of monovacancy are found to play an important role in the contribution to the total diffusion coefficient at temperatures above 2/3 of T_m, which could be one of the reasons of the upward curvature of the Arrhenius diagram in tungsten self-diffusion experiments. The diffusion pre-exponential factor for monovacancy diffusion is found to be two to three orders of magnitude higher than commonly used in computational studies, resulting in an attempt frequency of the order of 10^{15} Hz. The use of this remarkably much higher jump frequency might have surprisingly large effects on the simulation results of different multi-scale models.

Publication III: Concentration dependent hydrogen diffusion in tungsten
T. Ahlgren and L. Bukonte, *Journal of Nuclear Materials* 479 (2016) 195.

In this article, we study the diffusion of H in tungsten as a function of temperature, H concentration and pressure by employing the molecular dynamics method. The diffusion coefficient of H is found to decrease with increasing H concentration due to the neighbouring interstitial site blocking and repulsion between H atoms. We present a new analysis method to determine the diffusion coefficient that accounts for the random oscillation of atoms around the equilibrium position. A more accurate H migration barrier of 0.25 eV is obtained in this study and should be used instead of the commonly accepted value of 0.39 eV.

Publication IV: Comparison of molecular dynamics and binary collision approximation simulations for atom displacement analysis
L.Bukonte, F. Djurabekova, J. Samela, K. Nordlund, S. A. Norris and M. J. Aziz, *Nuclear Instruments and Methods in Physics Research Section B* 297 (2013) 23 – 28.

The aim of this publication is to compare two simulation methods, molecular dynamics (MD) and binary collision approximation (BCA). The predictions of BCA and MD simulations for displacement cascades in amorphous and crystalline silicon and BCC tungsten by 1 keV Ar ion bombardment are compared. The results reveal a significant shortcoming of the BCA approach when applied to materials that are amorphous or become amorphous during ion irradiation. For the conditions reported in this article, BCA agrees with MD simulation results at displacements larger than 5 Å, whereas at smaller displacements a difference between BCA and MD arises due to large amount of small displacements observed in MD simulations, but absent from a regular BCA approach due to the algorithm limitations.

2.2 Author's Contribution

The author developed a theoretical thermodynamics model to estimate the equilibrium vacancy fraction in metals accounting for the presence of interstitial impurities for Publication **I**, obtained and analyzed the results. The author employed the molecular dynamics method to simulate vacancy diffusion in Publication **II** and analyzed the results. For Publication **III**, the

author contributed to the MD simulations by finding the correct H positions in the crystal lattice and, by fitting, obtained the equation for the concentration dependent diffusion coefficient. The author carried out all molecular dynamics and binary collision approximation simulations for Publication **IV**, compared and analyzed the results obtained by both methods. Publications **I**, **II** and **IV** are written by the author of this thesis. In Publication **III**, the authour contributed to the conclusions of the presented work.

2.3 Other Scientific Work

The author has also contributed to the following publications in related scientific fields. These, however, are not discussed in detail in this thesis.

[1] MD-Predicted Phase diagrams for Pattern Formation
S. A. Norris, J. Samela, C. S. Madi, M. P. Brenner, L. Bukonte, M. Backman, F. Djurabekova, K. Nordlund and M. J. Aziz, *Nature communications* 2, 276 (2011).

[2] Mechanism of vacancy formation induced by hydrogen in tungsten
Y.-N. Liu, T. Ahlgren, L. Bukonte, K. Nordlund, X. Shu, Y. Yu, Guang-Hong and X.-C. Li, *AIP Advances* 3, 122111 (2013).

[3] The relationship between gross and net erosion of beryllium at elevated temperature
R. P. Doerner, I. Jepu, D. Nishijima, E. Safi, L. Bukonte, A. Lasa, K. Nordlund and T. Schwarz-Selinger, *Journal of Nuclear Materials* 463 (2015), 777.

[4] Sink strength simulations using the Monte Carlo method: applied to spherical traps
T. Ahlgren, L. Bukonte, *submitted for publication in Journal of Nuclear Materials*

Chapter 3

Theoretical Background on Thermodynamics of Defects

3.1 Defect formation

Crystal with no intrinsic defects are highly improbable in temperatures above absolute zero. The presence of defects in the crystalline lattice may greatly influence the properties of the material, therefore, studying the formation and migration mechanisms of various defects and estimating their concentration is of crutial importance. Despite the fact that the creation of a defect in a crystal lattice requires energy, there is also a gain in the entropy upon the formation of a defect. Defects continue to increase in their concentration until the free energy of the system has reached its minimum. According to thermodynamics [5–7], the change of the Gibbs energy, ΔG at temperature T is associated with the change in enthalpy, ΔH, and the change in entropy, ΔS, of the crystal by the following equation:

$$\Delta G = \Delta H - T\,\Delta S. \tag{3.1}$$

The enthalpy of a system is the sum of the internal energy and the product of pressure and volume of the system ($H = E + PV$). At zero pressure the enthalpy and the total energy of the crystal are equivalent quantities. To the first approximation the change in the enthalpy is proportional to the number of defects formed. Assuming the crystal contains only monovacancies, the change in the total enthalpy of the system can be written as:

$$\Delta H = \Delta H^{v_1} = N^{v_1}\, E_f^{v_1}, \tag{3.2}$$

where ΔH^{v_1} is the change of the total enthalpy of a system containing only monovacancies, $E_f^{v_1}$ is the monovacancy formation energy and N^{v_1} is the number of monovacancies.

The monovacancy formation energy, $E_f^{v_1}$, is the energy required to create a vacancy in the system near the surface, and is calculated as the difference between the energy of a system containing one vacancy, E^{N^0-1}, and the energy of a perfect crystal, E^0, [8]:

$$E_f^{v_1} = E^{N^0-1} - \left(\frac{N^0-1}{N^0}\right) E^0, \tag{3.3}$$

where N^0 is the number of host atoms.

The total entropy term, ΔS, consists of the vibrational entropy, ΔS_{vib}, and the configurational entropy, ΔS_{conf}, as well as the electronic and magnetic entropy, the two later being neglected in this thesis due to the small effect on the total entropy. The vibrational entropy describes random vibrational motion in a defected crystal and is also proportional to the number of defects formed:

$$\Delta S_{vib} = N^{v_1} \Delta S_{vib}^{v_1}. \tag{3.4}$$

The configurational entropy, on the other hand, has a probabilistic nature, and is associated with the defect distribution in the lattice. The configurational entropy is the main reason for defect presence in a crystal lattice. Having a crystal with no intrinsic defects at equilibrium is highly improbable, whereas, for example, vacancies give rise to many lattice configurations with different energy states. The increasing amount of defects results in higher configurational entropy and, as a consequence, in the lowering of the Gibbs free energy of the system. The configurational entropy of the system depends on the statistical weight, Ω, that describes the permutation of defect distribution in the crystal lattice. Again assuming that the crystal contains only monovacancies – the number of possible ways isolated monovacancies can reside in $N^{latt} = N^0 + N^{v_1}$ sites is:

$$\Omega^{v_1} = \frac{N^{latt}!}{N^0!\, N^{vac}!} = \frac{(N^0 + N^{v_1})!}{N^{v_1}! N^0!}, \tag{3.5}$$

where N^{latt} is the number of lattice sites.

According to the Boltzmann's definition of entropy, the total configurational entropy of the system is written as:

$$\Delta S_{conf} = k_B \ln \Omega^{v_1}. \tag{3.6}$$

Using the Stirling's formula: $log(A!) \approx A\,log(A) - A$, the Eq. (3.6) takes the form:

$$\Delta S_{conf} = k_B \left(N^0 \ln \frac{N^0 + N^{v_1}}{N^0} + N^{v_1} \ln \frac{N^0 + N^{v_1}}{N^{v_1}} \right). \tag{3.7}$$

Combining Eqs. (3.1), (3.2), (3.4) and (3.7) results in:

$$\Delta G = N^{v_1}\, E_f^{v_1} - T\, N^{v_1} \Delta S_{vib}^{v_1} + k_B T \left(N^0 \ln \frac{N^0 + N^{v_1}}{N^0} + N^{v_1} \ln \frac{N^0 + N^{v_1}}{N^{v_1}} \right). \tag{3.8}$$

Using the equilibrium condition:

$$\frac{\partial \Delta G}{\partial N^{v_1}} = 0, \tag{3.9}$$

and rearranging the equation, results in:

$$\frac{N^{v_1}}{N^0 + N^{v_1}} = \exp\left(\frac{-E_f^{v_1}}{k_B T}\right) \cdot \exp\left(\frac{\Delta S_{vib}^{v_1}}{k_B}\right). \tag{3.10}$$

This is the equation for estimating the monovacancy fraction in the pure crystal at thermodynamic equilibrium.

It is known that the presence of impurity can enhance vacancy formation due to trapping in vacancies [9, 10]. This phenomena is called superabundant vacancy formation (SAV) and can be quantitatively estimated by applying thermodynamic theory as follows. The impurity atoms, N^{imp}, present in a crystal can be located at interstitial sites (IS), also called solution sites, whereas others are trapped in the vacancies, i.e., reside in the trapping sites (TS). If there is an attraction between impurity atoms and a vacancies, the vacancies can usually trap several

impurity atoms. The binding energy E_b for the nth trapped impurity is the energy needed to remove it from the vacancy and place it on an IS, and is expressed as:

$$E_b = [E(n-1) + E^1] - [E(n) + E^0], \tag{3.11}$$

where $E(n-1)$ is the energy of the system, where $(n-1)$ impurities are in the vacancy, and E^1 is the energy with one impurity in an IS, $E(n)$ is the energy of the system, where n impurities are in the vacancy and E^0 is the energy of the reference system.

If the binding energy is positive, energy is gained when an additional impurity is trapped in the vacancy. The binding energy for each additional impurity usually depends on the number of impurities already occupying the vacancy. The cumulative binding energy for n impurities in a vacancy can be very generally expressed by a polynomial function of n:

$$E_b^{cum}(n) = \sum_{i=1}^{n} E_b(i) = (a\,n^3 + b\,n^2 + c\,n), \tag{3.12}$$

where a, b and c are fitting constants (presented in Publication **I** for systems studied in this thesis and shown to give a good fit to the binding energies obtained from the first principle studies).

To find the enthalpy change, ΔH^{imp}, when impurity atoms are trapped in the vacancies we define the number of trapped impurities as:

$$N_{tr}^{imp} = n_1\,N^{v_1}, \tag{3.13}$$

where n_1 is the number of trapped impurities in one monovacancy. The enthalpy change of the system when N_{tr}^{imp} impurity atoms are trapped in N^{v_1} is:

$$\Delta H^{imp} = -N^{v_1}\,(A\,n_1^3 + B\,n_1^2 + C\,n_1), \tag{3.14}$$

where A, B, C are the fitting parameters of H cumulative binding energy to a monovacancy. Then the total enthalpy change of the system with N^{v_1} vacancies and N_{tr}^{imp} trapped impurity atoms becomes:

$$\Delta H = \Delta H^{v_1} + \Delta H^{imp} = N^{v_1}\,[E_f^{v_1} - (A\,n_1^3 + B\,n_1^2 + C\,n_1)]. \tag{3.15}$$

The enthalpy of the vacancy formation is decreased due to the energy gained when impurity atoms from the IS are trapped in the vacancies.

The interstitial or trapping site occupancy of impurity atoms can considerably change the vibrational entropy value. The vibrational entropy associated with impurities, ΔS_{vib}^{imp1}, is proportional to vacancies formed in the host material since it is the difference in the vibrational entropy between IS and TS occupancy of the impurity atoms. The total vibrational entropy change when N^{v_1} vacancies are formed in a crystal with n_1 impurities per vacancy can be written as:

$$\Delta S_{vib} = N^{v_1} \left(\Delta S_{vib}^{v_1} + n_1 \Delta S_{vib}^{imp1} \right). \tag{3.16}$$

The total statistical weight to distribute defects in a crystal lattice becomes:

$$\Omega^{tot} = \Omega^{v_1} \, \Omega^{trap1} \, \Omega^{int}, \tag{3.17}$$

where Ω^{trap1} is the number of ways to distribute $n_1 \, N^{v_1}$ trapped impurities among total number of trapping sites $n_1^{max} \, N^{v_1}$ (n_1^{max} being the maximum number of impurities one monovacancy can accommodate):

$$\Omega^{trap1} = \frac{(n_1^{max} \, N^{v_1})!}{(n_1 \, N^{v_1})! (n_1^{max} \, N^{v_1} - n_1 \, N^{v_1})!}, \tag{3.18}$$

and Ω^{int} is the number of ways to distribute $N^{imp} - n_1 \, N^{v_1}$ residual impurity atoms among all interstitial sites ($m \, N^0$) in the crystal lattice, where m is the number of IS per host atom:

$$\Omega^{int} = \frac{(m \, N^0)!}{(N^{imp} - n_1 \, N^{v_1})! \; (m \, N^0 - (N^{imp} - n_1 \, N^{v_1}))!}. \tag{3.19}$$

For convenience, we express the system parameters as fractions:

Fraction of monovacancies:	$[V_1]$	$=$	$\frac{N^{v_1}}{N^0}$
Fraction of divacancies:	$[V_2]$	$=$	$\frac{N^{v_2}}{N^0}$
Fraction of impurities:	$[I]$	$=$	$\frac{N^{imp}}{N^0}$
Fraction of impurities in IS:	$[I_{IS}]$	$=$	$\frac{N_{IS}^{imp}}{N^0}$
Total fraction of vacancies:	$[V_{tot}]$	$=$	$[V_1] + 2\,[V_2]$

where N_0 is the number of host atoms.

Following the equilibrium condition and minimizing the Gibbs free energy of the system, the final system of equations is obtained:

$$\begin{cases} \frac{E_f^{v_1} - (A\,n_1^3 + B\,n_1^2 + C\,n_1)}{k_B T} - \frac{(\Delta S_{vib}^{v_1} + n\,\Delta S_{vib}^{imp1})}{k_B} = \ln\left(\frac{1}{[V_1]} + 1\right) - n_1^{max}\,\alpha + n_1\,M & (3.20) \\ \frac{-\left(3\,A\,n_1^2 + 2\,B\,n_1 + C\right)}{k_B T} - \frac{\Delta S_{vib}^{imp1}}{k_B} = M & (3.21) \end{cases}$$

where $M = \ln\left(\frac{[I_{IS}]}{m - [I_{IS}]}\right)$ and $\alpha = \ln\left(\frac{n_1^{max} - n_1}{n_1}\right)$.

Using this set of equations it is possible to estimate the monovacancy fraction in a crystal in the presence of impurities.

Depending on the material properties and impurity amounts, divacanies and larger vacancy clusters may considerably contribute to the total equilibrium vacancy fraction and need to be taken into consideration. Following the procedure above, a system of equations for calculating the total vacancy fraction including the thermodynamics of monovacancies and divacancies, as well as the entropy and impurity binding parameters, is obtained as:

$$\begin{cases} \frac{(E_f^{v_2} - E\,n_2^3 - F\,n_2^2 - G\,n_2)}{k_B T} - \frac{(\Delta S_{vib}^{v_2} + n_2 \Delta S_{vib}^{imp2})}{k_B} = & (3.22) \\ = \ln\left(\frac{(L - [V_2])}{[V_2]}\right) + n_2\,\beta + z\,\ln(\frac{L}{(L - [V_2])}) + n_2\,M - n_2^{max}\,\beta & \\ \frac{(E_f^{v_1} - A\,n_1^3 - B\,n_1^2 - C\,n_1)}{k_B T} - \frac{(\Delta S_{vib}^{v_1} + n_1 \Delta S_{vib}^{imp1})}{k_B} = & (3.23) \\ = \ln(\frac{1}{[V_1]} + 1) + n_1\,\alpha + n_1\,M + \frac{z}{2}\ln(\frac{L}{(L - [V_2])}) - n_1^{max}\,\alpha & \\ -\frac{\Delta S_{vib}^{imp1}}{k_B} - \frac{(3\,A\,n_1^2 + 2\,B\,n_1 + C)}{k_B T} = \alpha + M & (3.24) \\ -\frac{\Delta S_{vib}^{imp2}}{k_B} - \frac{(3\,E\,n_2^2 + 2\,F\,n_2 + G)}{k_B T} = \beta + M & (3.25) \end{cases}$$

where $L = \frac{z}{2}\,(1 + 2\,[V_2] + [V_1])$, $\beta = \ln(\frac{(n_2^{max} - n_2)}{n_2})$, $E_f^{v_2}$ is the divacancy formation energy, E, F, G are the fitting parameters for impurity binding to the divacancy, $\Delta S_{vib}^{v_2}$ is the change in the vibrational entropy of the divacancy formation, n_2 - impurities trapped per divacancy, ΔS_{vib}^{imp2} vibrational entropy change of impurity atom occupancy in IS sites and TS in divacancy and z is the configurational factor associated with the divacancy.

This set of equations (3.22 - 3.25) is utilized in Publication **I** to estimate the total equilibrium vacancy fraction in four metals (Pd, Ni, Co, Fe) in correlation with varying H amounts. The results are compared with the experimental data and further discussed in Chapter 6.1.

3.2 Defect diffusion

In crystal at finite temperatures each atom resides in its lattice position and oscillates around its equilibrium position with some frequency ν. Occasionally, given enough thermal energy, these oscillations may become large enough for a particle to overcome the energy barrier, arising from the bond breaking with neighbouring atoms and lattice distortions, and change the lattice site. This process can be characterized by the change in the Gibbs free energy of migration, ΔG_m, representing the free energy difference between the equilibrium position and the activated state with the largest energy – the saddle point [11]:

$$\Delta G_m = \Delta H_m - T\Delta S_m + P\Delta V_m, \tag{3.26}$$

where ΔH_m is the change in the enthalpy of migration, ΔS_m is the change in the entropy of migration, P is pressure and ΔV_m is the migration volume. The migration volume is the volume change when the diffusing particle is transferred from its equilibrium position to the saddle point. The enthalpy of migration ΔH_m denotes the height of the energy barrier a particle needs to overcome for a diffusion jump to occur.

The change in the migration entropy, ΔS_m, corresponds to the difference in lattice vibrations at the equilibrium position and the saddle point:

$$\Delta S_m = k_B \left[\sum_{j\neq 0}^{3N-1} \ln\left(\frac{h\nu_j}{k_B T}\right) - \sum_{j\neq 0}^{3N-1} \ln\left(\frac{h\nu'_j}{k_B T}\right) \right], \tag{3.27}$$

where v_j are the $3N-1$ normal mode frequencies for vibrations around the equilibrium position, v'_j are the frequencies for the saddle point configuration, having one real normal mode less than the frequencies at the equilibrium site, because the negative curvature of energy landscape leads to one imaginary frequency in the direction of a jump, and h is Plank's constant.

According to the rate theory [12] an average jump frequency of a particle to move from one lattice position to a neighbouring one, assuming the pressure is small or the migration volume is zero, is:

$$w = \nu_0 \exp\left(\frac{-\Delta G_m}{k_B T}\right) = \nu_0 \exp\left(\frac{\Delta S_m}{k_B}\right) \exp\left(\frac{-\Delta H_m}{k_B T}\right), \tag{3.28}$$

where ν_0 is the attempt frequency for diffusion jump. The $\exp\left(\frac{-\Delta H_m}{k_B T}\right)$ term is the "Boltzmann factor" that gives the probability for the diffusing particle to have an energy ΔH_m at temperature T. In the harmonic approximation, the attempt frequency is expressed as:

$$\nu_0 = \frac{\prod_{i=1}^{3N} v_j}{\prod_{i=1}^{3N-1} v_j'}. \tag{3.29}$$

It is usually assumed to be of the order of the Debye frequency [13].

Depending on the diffusion mechanism and material under the consideration these equations can take slightly different forms, however, the main principle of the jumping process stays the same.

One can distinguish between several diffusion mechanisms – the most common of them being vacancy diffusion and interstitial diffusion. If a lattice atom moves from its position to a neighbouring empty lattice site, it is said that an atom has diffused via the vacancy mechanism. If the crystal contains impurity atoms that reside in the interstitial positions and move from one interstitial position to another without permanently displacing the host atoms, it is called the interstitial mechanism of diffusion.

Other diffusion mechanisms exist. As an example, self-interstitial diffusion in BCC metals usually occur by the collective motion of atoms along the $\langle 111 \rangle$ direction, this is called the crowdion mechanism. In the case of semiconductors the diffusion is more complex. The charge of the moving defect plays an important role in the diffusion process. For example, if a vacancy is an electron acceptor, the diffusion coefficient would increase in the n-type semiconductor and decrease in the p-type semiconductor [14]. These complex diffusion mechanisms in semiconductors, however, are not discussed in more detail in this thesis.

For atom diffusion via the vacancy mechanism, the probability for an atom to make a jump can be expressed as a product of the jump frequency (or jump rate) and the probability that the site next to it is vacant:

$$\Gamma = Z\, w\, [V_1] = Z\, \nu_0 \exp\left(-\frac{\left[\Delta H_f^{v_1} + \Delta H_m^{v_1}\right]}{k_B T}\right) \exp\left(\frac{\Delta S_f^{v_1} + \Delta S_m^{v_1}}{k_B}\right), \tag{3.30}$$

where Z is the coordination number (in the case of diffusion via the vacancy mechanism it is the number of atoms adjacent to a vacancy). The diffusion through the vacancy mechanism is the dominating mechanism of self-diffusion in most metals and substitutional alloys.

When considering the interstitial diffusion mechanism for a dilute solution of foreign atoms assuming that the neighbouring interstitial sites are unoccupied, the total jump rate can be written as:

$$\Gamma = Z\, w = Z\, \nu_0 \exp\left(-\frac{\Delta H_m^{v_1}}{k_B T}\right) \exp\left(\frac{\Delta S_m^{v_1}}{k_B}\right), \tag{3.31}$$

where Z is the number of nearest neighbour interstitial sites of the same type.

To derive the diffusion coefficient it is useful to consider a concentration C of particles located in plane x at time $t + \tau$. At time t these particles were located in the planes $x - X$, where X is the displacement of the particles [11]. The balance equation for the number of particles can be written as:

$$C(x, t + \tau) = \sum_X C(x - X, t) \cdot W(X, \tau), \tag{3.32}$$

where $W(X, \tau)$ is the distribution function, which denotes the probability that after a time τ a particle will have travelled a path X along the x-axis, where the sum is done over all values of X. The explicit form of the distribution function is not needed in this derivation.

Expanding the left hand side of the above equation in a Taylor series for the small time step τ, we obtain:

$$C(x, t + \tau) = C(x, t) + \tau \frac{\delta C}{\delta t} + ... \tag{3.33}$$

For small τ the higher order terms become negligible.

Using the Taylor series on the concentration term on the right hand side of the equation, expanding around $X = 0$:

$$\sum_X C(x - X, t) \cdot W(X, \tau) = \tag{3.34}$$
$$\sum_X \left[C(x,t) - X\frac{\delta C}{\delta x} + \frac{X^2}{2}\frac{\delta^2 C}{\delta x^2} + ... \right] \cdot W(X, \tau).$$

It is useful to introduce:

$$\sum_X W(X, \tau) = 1 \tag{3.35}$$

$$\sum_X X^n W(X, \tau) = \langle X^n \rangle , \tag{3.36}$$

where the first equation states that the probabilities are normalized, and the second defines the n^{th} moments of X.

For the limit $\tau \longrightarrow 0$ the probability distribution function becomes localized at point $x = 0$, therefore, terms higher than the second order in Eq. (3.34) can also be omitted.

Combining these equations and cancelling the common term $C(x, t)$, the balance equation becomes:

$$\frac{\delta C}{\delta t} = -\frac{\langle X \rangle}{\tau}\frac{\delta C}{\delta x} + \frac{\langle X^2 \rangle}{2\tau}\frac{\delta^2 C}{\delta x^2}. \tag{3.37}$$

For a random walk with the absence of driving force $\langle X \rangle = 0$, the equation reduces to the one dimensional diffusion equation:

$$\frac{\delta C}{\delta t} = \frac{\langle X^2 \rangle}{2\tau}\frac{\delta^2 C}{\delta x^2}, \tag{3.38}$$

with the definition of the diffusion coefficient:

$$D \equiv \frac{\langle X^2 \rangle}{2\tau}. \tag{3.39}$$

This expression relates the diffusion coefficient to the mean square displacement in the x direction. Since the total displacement of a diffusing particle after many individual displacements is composed of its X, Y and Z components as $R^2 = X^2 + Y^2 + Z^2$, then for cubic crystals and

isotropic medium ($\langle X^2\rangle = \langle Y^2\rangle = \langle Z^2\rangle = \frac{1}{3}\langle R^2\rangle$) the three dimensional diffusion coefficient becomes:

$$D \equiv \frac{\langle R^2\rangle}{6\tau}. \tag{3.40}$$

This is called the *Einstein−Smoluchowski* relation [15]. A modified *Einstein−Smoluchowski* equation is used in Publications **II** and **III** to calculate the diffusion coefficient for monovacancies and H atoms in tungsten.

The monovacancy diffusion in tungsten is studied in Publication **II** in order to address the unresolved question of the reasons for the increase of the diffusion coefficient at temperatures above 2/3 of T_m observed in tungsten self-diffusion experiments [16]. The H diffusion in tungsten is studied in Publication **III**. An analytical form for the concentration dependent diffusion coefficient is proposed and the reasons for the decrease of diffusion coefficient with increasing H concentration are discussed.

Diffusion in cubic crystals

From the microscopic point of view, the diffusion can be thought of as a random walk problem. The displacement of the diffusing particle in one dimension can be expressed as a sum of the individual jump projections on the x-axis:

$$X = x_1 + x_2 + ... + x_n = \sum_{i=1}^{n} x_i. \tag{3.41}$$

The mean squared displacement is averaged over an ensemble of diffusing particles:

$$\langle X^2\rangle = \sum_{i=1}^{n}\langle x_i^2\rangle + 2\sum_{i=1}^{n-1}\sum_{j=i+1}^{n}\langle x_i x_j\rangle\,. \tag{3.42}$$

The first term contains only the average squared magnitude of each jump separately. The second term is a product of two subsequent jumps, and it is said to contain a memory of the walk. If the jumps are truly random and, thus, uncorrelated, the root mean square displacement takes a form containing no double sums ($\langle x_i x_j\rangle$ cancel out when an average is taken over a large number of particles)

$$\left\langle X^2 \right\rangle = \sum_{i=1}^{n} \left\langle x_i^2 \right\rangle . \tag{3.43}$$

In crystalline solids diffusion is usually mediated by the lattice defects, such as vacancies and interstitials. These defects move in a lattice towards definite directions s with the discreate jump length. The total number of jumps n is made from n_s jumps in the s direction, where s ranges from 1 to Z amd Z is the coordination number of a crystal. The projected length of n_s jump on x-axis is x_s. The mean squared displacement in the x-direction can be written as follows:

$$\left\langle X^2 \right\rangle = \sum_{i=1}^{n} \left\langle x_i^2 \right\rangle = \sum_{s=1}^{Z} \langle n_s \rangle x_s^2. \tag{3.44}$$

Introducing the average jump frequencies as $\Gamma_s \equiv \langle n_s \rangle / \tau$ of the type s, the mean squared displacement becomes:

$$\left\langle X^2 \right\rangle = \tau \sum_{s=1}^{Z} \Gamma_s x_s^2. \tag{3.45}$$

Combining Eq. (3.45) with the one dimensional $Einstein-Smoluchowski$ relation, the diffusion coefficient in x-direction is expressed as:

$$D_x = \frac{1}{2} \sum_{s=1}^{Z} \Gamma_s x_s^2. \tag{3.46}$$

This equation is used to obtain the diffusion in crystalline solids when diffusing via definite lattice sites.

For cubic crystals the jump rate Γ_s is a constant, i.e., it is independent of jump type s ($D_x = D_y = D_z = D$) and the total jump rate is $\Gamma = Z \cdot \Gamma_s$:

$$D = D_x = \frac{1}{2}\Gamma_s \sum_{s=1}^{Z} x_s^2 = \frac{1}{2\,Z}\Gamma \sum_{s=1}^{Z} x_s^2. \tag{3.47}$$

The diffusion coefficient in terms of the jump length λ in 3 dimension:

$$D = \frac{1}{6}\Gamma_s \sum_{s=1}^{Z} \lambda^2 = \frac{\Gamma}{6\,Z} \sum_{s=1}^{Z} \lambda^2. \tag{3.48}$$

If the jump length λ is the same in all s type jumps, we finally get:

$$D = \frac{1}{6}\Gamma\lambda^2. \tag{3.49}$$

This equation, Eq. (3.49), is valid for all cubic structures with nearest neighbour jumps. To justify this statement, the diffusion coefficients for BCC and FCC structures are derived as follows.

Diffusion in a BCC lattice.

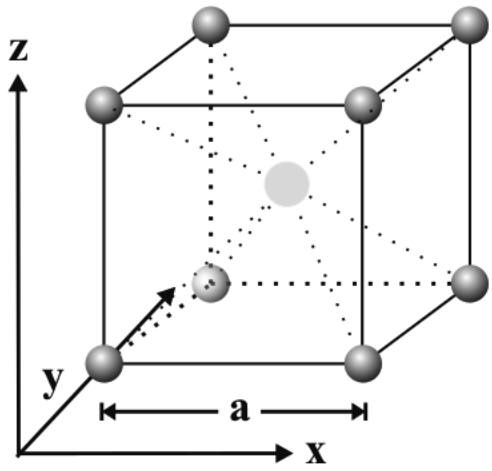

Figure 3.1: Monovacancy (in the middle) in the BCC lattice.

In a BCC crystal with a lattice constant a, an atom has $Z = 8$ jump directions (Fig. 3.1), each with the projected length $\pm a/2$ on the x-axis, same projections to y and z-axis. Using Eq. (3.47), we get:

$$D = D_x = \frac{1}{2 \cdot 8}\Gamma\left[8\left(\frac{a}{2}\right)^2\right] = \frac{\Gamma}{8}a^2. \tag{3.50}$$

Using the jump length $\lambda = \sqrt{3}a/2$, gives $a = 2\lambda/\sqrt{3}$, which when inserted into Eq. (3.50) gives:

$$D = \frac{\Gamma}{8}\left[\frac{4\lambda^2}{3}\right] = \frac{\Gamma}{6}\lambda^2. \tag{3.51}$$

Diffusion in a BCC lattice through tetrahedral interstitial sites.

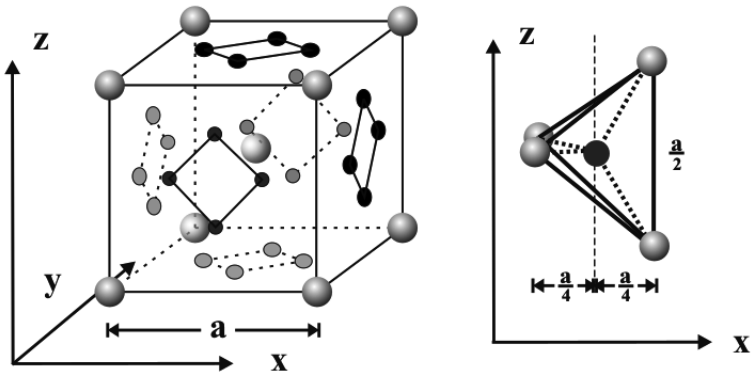

Figure 3.2: On the left: The BCC lattice with four tetrahedral interstitial sites of each of the six cell faces. On the right: the tetrahedral interstitial site with four nearest neighbour host atoms.

In a BCC lattice there are four nearest neighbour tetrahedral interstitial sites ($Z = 4$), shown in Fig. 3.2. The distance (jump length) between these sites is $\lambda = a/\sqrt{8}$. The interstitials occupying the tetrahedral sites do not move from one interstitial position to another with equal projections in all directions, thus the diffusion coefficient must be obtained by examining each direction separately. The tetrahedral interstitial jumps in the BCC lattice: all four possible jumps move in the x direction with the projection $a/4$, two of these jumps move also in the z direction with the projection $a/4$, having y projection 0 and the other two jumps have a y projection $a/4$ with z projection equal to 0.

Employing the Einstein–Smoluchowski relation, Eq. (3.39), with:

$$\left\langle X^2 \right\rangle = \tau \sum_{s=1}^{4} \Gamma_s x_s^2 = \tau \left[\Gamma_s \frac{a^2}{16} + \Gamma_s \frac{a^2}{16} + \Gamma_s \frac{a^2}{16} + \Gamma_s \frac{a^2}{16} \right] = 4 \cdot \tau \left[\Gamma_s \frac{a^2}{16} \right], \tag{3.52}$$

$$\left\langle Y^2 \right\rangle = \tau \sum_{s=1}^{4} \Gamma_s y_s^2 = \tau \left[\Gamma_s \frac{a^2}{16} + \Gamma_s \frac{a^2}{16} + 0 + 0 \right] = 2 \cdot \tau \left[\Gamma_s \frac{a^2}{16} \right], \tag{3.53}$$

$$\left\langle Z^2 \right\rangle = \tau \sum_{s=1}^{4} \Gamma_s z_s^2 = \tau \left[0 + 0 + \Gamma_s \frac{a^2}{16} + \Gamma_s \frac{a^2}{16} \right] = 2 \cdot \tau \left[\Gamma_s \frac{a^2}{16} \right]. \tag{3.54}$$

Equation (3.40) gives:

$$D = \frac{\langle R^2 \rangle}{6\tau} = \frac{\langle X^2 \rangle + \langle Y^2 \rangle + \langle Z^2 \rangle}{6\tau} = \frac{\tau 8 \Gamma_s \, a^2}{6\tau \, 16} = \frac{\Gamma_s \, a^2}{12}. \tag{3.55}$$

Since the total jump rate $\Gamma = 4\,\Gamma_s$ and $\lambda = a/\sqrt{8}$, the diffusion coefficient is:

$$D = \frac{\Gamma \, a^2}{4 \cdot 12} = \frac{\Gamma \, 8 \, \lambda^2}{4 \cdot 12} = \frac{\Gamma \, \lambda^2}{6}. \tag{3.56}$$

The diffusion coefficient in an FCC crystal through octahedral interstitial sites.

In an FCC crystal there are 12 neighbouring octahedral sites for an interstitial impurity atom (Z = 12). The octahedral interstitial sites in an FCC lattice are shown in Fig. 3.3. Four of these diffusion jumps are perpendicular to the x-axis (the projection being 0) and eight jumps have projected lengths $\pm a/2$ on the x-axis. The diffusion coefficient, according to Eq. (3.47), with a jump length $\lambda = a/\sqrt{2}$, again becomes the same as Eq. 3.49:

$$D_x = D = \frac{\Gamma}{2 \cdot 12} \left[4 \cdot 0 + 8 \frac{a^2}{4} \right] = \frac{\Gamma}{12} a^2 = \frac{\Gamma}{6} \lambda^2. \tag{3.57}$$

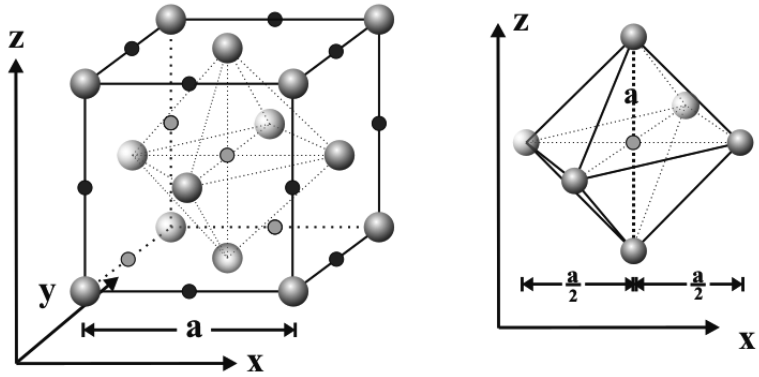

Figure 3.3: On the left: an FCC lattice with octahedral interstitial sites. On the right: an octahedral interstitial site with six nearest neighbour host atoms.

Correlation effects

In the previous section the expression for diffusion coefficient was derived and given in Eq. (3.40), which relates the mean squared displacement to the diffusion coefficient. $\langle R^2 \rangle$ consists of two terms: the first term represents a random walk, whereas the second term is a product between two subsequent jumps and if the diffusion process is correlated, this term is no longer zero:

$$\left\langle R^2 \right\rangle = \sum_{i=1}^{n} \left\langle r_i^2 \right\rangle + 2 \sum_{i=1}^{n-1} \sum_{j=i+1}^{n} \left\langle r_i r_j \right\rangle . \tag{3.58}$$

For example, in a dilute solution of interstitials among the host atoms, there is a high probability that the neighbouring interstitial sites are available and therefore there is no correlation between the diffusion jumps. However, if the concentration of interstitial atoms is high, the mobility of particles is limited due to site blocking. The interstitial atom cannot jump to one or several interstitial sites because they are already occupied. Then the diffusion path depends on the local environment and it can be accounted for by introducing a correlation factor f [11]:

$$f = \lim_{n\to\infty} \frac{\langle R^2 \rangle}{\langle R^2_{random} \rangle} = 1 + 2 \lim_{n\to\infty} \frac{\sum_{i=1}^{n-1} \sum_{j=i+1}^{n} \langle r_i r_j \rangle}{\sum_{i=1}^{n} \langle r_i^2 \rangle} \tag{3.59}$$

The diffusion coefficient then should be modified as follows:

$$D = \frac{1}{6} f \Gamma \lambda^2. \tag{3.60}$$

If $f = 1$ the diffusion is random, if $f < 1$ diffusion is said to have correlation effects.

Chapter 4

Theoretical Background on Irradiation Effects in Solids

Ion irradiation is a process often used to study and alter the physical, chemical and electrical properties of materials. Understanding the events taking place when an energetic ions interacts with a material have been of a crucial interest for technological purposes. Ion implantation has been widely used, for example, in semiconductor doping, which is the basis of nearly all modern electronic devices. Each implanted ion entering the material and interacting with the target atoms loses energy until it stops completely at some depth. The stopping power, S, for this particle is a measure of the average energy loss per unit path length:

$$S = \frac{dE}{dx}, \tag{4.1}$$

where dE is the kinetic energy change and dx is the path of the particle along its trajectory.

At high ion energies (above ≈ 10 keV/u) a charged particle mostly undergoes a process called electronic stopping that occurs due to inelastic collisions between the ion and bound electrons in the medium. At lower energies the entering ion loses its energy mainly due to collisions with target atoms. This process, called nuclear stopping, is elastic and can be described by classical kinematics. The classical transfer of energy between a moving and a stationary particle depends on the mass and charge of both particles and the velocity of the incident ion. When the moving particle impacts the stationary particle, the stationary particle is displaced from its initial position due to the energy transfer and the moving particle is deflected. Since it is an elastic process, the energy and the momentum of the system is conserved, the energy transfer T from

a projectile to the stationary atoms can be written as [17]:

$$T = \frac{4m_1 \cdot m_2}{(m_1 + m_2)^2} E_0 \sin^2 \frac{\Theta}{2} = T_{max} \sin^2 \frac{\Theta}{2}. \tag{4.2}$$

This is also the energy for a recoil ion in the binary collision approximation (BCA) simulations. The maximum transfer of energy occurs when the angle $\Theta = 180^o$ is called a head-on collision.

The scattering angle of deflection in the spherically symmetric potential can be expressed as [18]:

$$\Theta = \pi - 2b \int_{-\infty}^{\infty} \frac{dr}{r^2 \left[1 - \frac{V(r)}{E_{cm}} - \frac{b^2}{r^2}\right]^{1/2}}. \tag{4.3}$$

This equation can be numerically integrated taking the limits of integration r_{min} and r_{max}, where r_{min} is the closest approach during the scattering event and can be found if the following condition is true:

$$\left[1 - \frac{V(r_{min})}{E_{cm}} - \frac{b^2}{r_{min}^2}\right] = 0 \tag{4.4}$$

and r_{max} can be chosen large enough, where the change of the integral is negligible. In practice the lower limit of intergration is chosen $r_{min} + \epsilon$, where *epsilon* is a small number.

The energy of the centre of mass coordinates expressed in terms of the energy in the laboratory frame is:

$$E_{cm} = \left(\frac{m_2}{m_1 + m_2}\right) E_{lab}. \tag{4.5}$$

Upon the irradiation of energetic particles, surface atoms can be ejected from a solid target, this process is called sputtering. It may happen when the energy transferred from a projectile to the target atoms is larger than the surface binding energy. The average number of sputtered atoms per incoming ion is called sputtering yield. It is an important parameter that depends on the ion incidence angle, the energy of the ion, the masses of the ion and the target atoms and the surface binding energy of the target material.

In order to permanently displace an atom from its initial lattice site to a defect position, the target atom must receive energy, Eq. (4.2), that is larger than the threshold displacement energy E_d of the material. The displacement energy can be expressed as a sum of the vacancy formation energy, the interstitial formation energy and the component that depends on the

surrounding lattice (mostly of the bond-bending). The lattice component arises due to the multi-body collision processes taking place in the collision cascade – an atom receiving the recoil energy can return to its lattice site or push a neighbouring atom into its place. Therefore, the average threshold displacement energy is typically much higher ($\sim$ 20 eV) than the Frenkel pair (vacancy–interstitial pair) formation energy ($\sim$ 5 - 10 eV) [19]. Threshold displacement energy depends on the crystallographic direction, hence very often the average displacement energy is used to describe the material. In irradiation processes the crystal orientation axes with respect to the surface is also important due to the channelling effects.

The irradiation effects on amourphous and crystalline silicon, and BCC tungsten are studied in Publication **IV**.

Chapter 5

Computational methods

5.1 Classical Molecular Dynamics

The molecular dynamics (MD) method is based on numerically solving the classical Newton's equations of motion of all the N particles present in the system:

$$F_i = m_i a_i, i = 1, 2, ...N, \tag{5.1}$$

where F_i denotes the force acting on each particle, m_i is the mass and a_i is the acceleration [20]. A simplified MD algorithm for atomistic simulations is shown in Fig. 5.1. Several numerical algorithms have been developed for integrating the equations of motion. The Verlet algorithm [21], for example, uses the Taylor expansion series to approximate the position, velocity and acceleration of all the particles. This method has the advantage of preserving the reversibility that is one of the most important properties of the Newton's equations. The error in the estimate of the position depends on the order of Taylor expansion. In applications where only the positions need to be calculated, this method has been proven to be very accurate and computationally efficient. However, normally in molecular dynamics simulations the velocities need to be calculated in order to compute, for example, the temperature and kinetic energy of the system. The velocities in the Verlet method are not explicitly solved. The error in the velocity calculation is, therefore, two orders of magnitude higher that in the estimate of the position. This leads to the main shortcoming of the Verlet method: energy fluctuations – the energy conservation rule might be violated.

Another, more accurate way to integrate numerically the equations of motion is the predictor – corrector algorithm. The predictor – corrector method is composed of three steps: prediction, evaluation, and correction. The predictor – corrector method first predicts the system

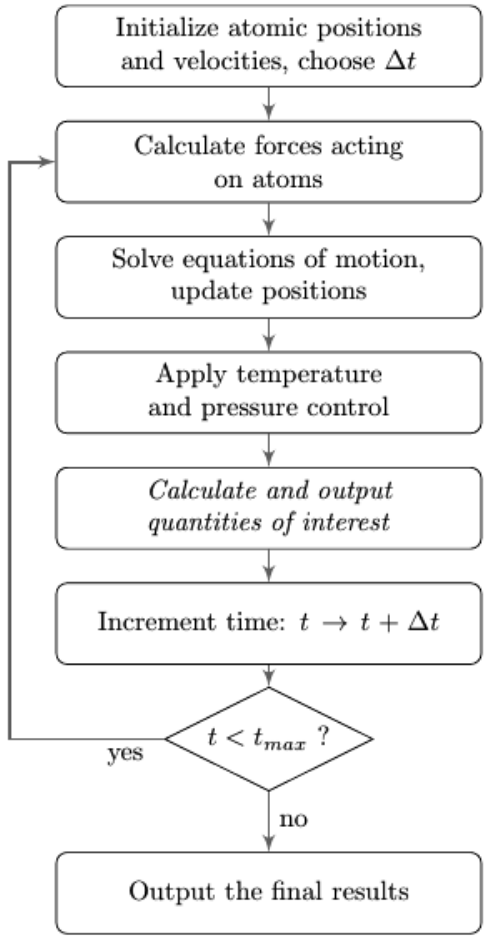

Figure 5.1: A simplified MD algorithm.

configuration at time $t + \Delta t$ using a Taylor expansion series:

$$\mathbf{r}^p(t + \Delta t) = \mathbf{r}(t) + \mathbf{v}(t)\Delta t + \frac{1}{2}\mathbf{a}(t)\Delta t^2 + \frac{1}{6}\mathbf{b}(t)\Delta t^3 + \frac{1}{24}\mathbf{c}(t)(\Delta t^4) + \frac{1}{120}\mathbf{d}(t)(\Delta t^5), \qquad (5.2)$$

where $\mathbf{r}$ is the position, $\mathbf{v}$ is the velocity, $\mathbf{a}$ is the acceleration and $\mathbf{b}$, $\mathbf{c}$, $\mathbf{d}$ are the higher order time derivatives of the position, the superscript p denotes the predicted configuration. The same procedure is carried out for the time derivatives of the position.

The forces are then evaluated at the new positions at the time $t + \Delta t$ to obtain the acceleration $\mathbf{a}(t + \Delta t)$. The differences between the predicted and calculated accelerations are calculated in order to obtain the error $\mathbf{\Delta a}(t + \Delta t)$ and the error is used to correct all the predicted positions

and their derivatives:

$$\mathbf{r}^c(t+\Delta t) = \mathbf{r}^p(t+\Delta t) + \mathbf{\Delta a}(t+\Delta t). \tag{5.3}$$

The corrections of the time derivatives are performed in the same manner.

The molecular dynamics code PARCAS (PARallel CAScade) [22] employed in this study, uses a Gear algorithm [25] based on the predictor– corrector method. The Gear method in addition to the predictor–corrector algorithm uses the set of coefficients c_i that are chosen depending on the order of the Taylor series expansion. The Gear algorithm is more accurate than the Verlet for short time steps, although the error increases more rapidly for longer time steps [20]. This method provides both the positions and velocities of the atoms at the same time and it can be used to calculate forces that depend explicitly on the velocity, this is indeed needed in algorithms which control temperature and pressure.

Molecular dynamics time step.
An important parameter in MD simulations is the integration time step Δt. It defines how often interactions between atoms in the system are calculated. The choice of Δt depends on the material and the nature of the simulation. To conserve the total energy of the system, the time step should be chosen to be about the magnitude of the fastest motion in the system. The atomic vibrational frequencies typically are of an order of 10^{13} Hz, which corresponds to 100 fs. However, during the simulations of energetic processes the atom displacements are much larger than in the thermal equilibrium simulation, as a consequence the time step needs to be chosen to be small enough to realistically describe the trajectories of fast moving atoms.

For computational efficiency, the MD code PARCAS uses the adaptive timestep [26]:

$$\Delta t_{n+1} = min\left(\frac{\Delta x_{max}}{v_{max}}, \frac{\Delta E_{max}}{F_{max} v_{max}}, c_{\Delta t}\Delta t_n, \Delta t_{max}\right), \tag{5.4}$$

where Δx_{max} is the maximum allowed distance at any time t, ΔE_{max} is the maximum allowed change in energy, v_{max} and F_{max} is the maximum speed of a particle and the maximum force that can act on it, respectively. The constant $c_{\Delta t}$ is chosen in such way that it prevents sudden changes in the time step and Δt_{max} is the time step for a system at equilibrium.

Temperature and pressure control
One common approach to control the temperature during the MD simulation is the Berendsen thermostat [27], which is based on a weak coupling between the system and an external bath.

In this method the velocities are scaled at each time step in such a way that the rate of change of temperature is proportional to the difference in temperature:

$$\frac{dT}{dt} = \frac{1}{\tau}(T_0 - T), \tag{5.5}$$

where τ is the coupling parameter that determines how tight is the coupling between the bath and the system, T_0 and T are desired and current temperature, respectively.

The temperature of a system is related to the kinetic energy of the particles in the system, therefore, the temperature can be easily altered by multiplying the velocities v by a factor λ:

$$\lambda = \left[1 + \frac{\Delta t}{\tau_T}\left(\frac{T_0}{T} - 1\right)\right]^{1/2}. \tag{5.6}$$

In a similar way as the temperature control, the Berendsen's pressure control is done by introducing a scaling factor μ to scale the size of the system and all atom coordinates:

$$\mu = \left[1 + \frac{\beta \Delta t}{\tau_P}\left(P_0 - P\right)\right]^{1/3}, \tag{5.7}$$

where β is the inverse of the bulk modulus of the system, P_0 is the desired pressure, P is the actual pressure of the system and τ_P is the time constant for pressure scaling.

5.1.1 Molecular Dynamics potential

MD allows us to follow the interactions of millions of atoms for up to microsecond time scales. To describe the atom interactions in MD simulation the analytical interatomic potentials are used. The forces between atoms are derived from the potential energy:

$$\vec{F_i} = -\nabla_r V(r_1, r_2, ..., r_N). \tag{5.8}$$

In general, the total potential energy of the system can be written as:

$$V_{tot} = \sum_{i}^{N} V_1(\vec{r_i}) + \sum_{i,j}^{N} V_2(\vec{r_i}\vec{r_j}) + \sum_{i,j,k}^{N} V_3(\vec{r_i}\vec{r_j}\vec{r_j}) + ..., \tag{5.9}$$

where V_1 is the one-body term that arises due to the external forces acting on the system or the boundaries of the cell. With no external forces $\sum_i^N V_1(\vec{r}_i)$ can be omitted. V_2 is the two-body term that includes the interaction for every pair in the system and its magnitude depends only on the interatomic distance between the pairs completely neglecting the influence of other atoms. V_3 is the three-body term which in addition to the pair interaction includes the effect of the third atom. A variety of interatomic potentials exist and the choice of it depends on the material and the nature of simulation. The requirements for a good interatomic potential are: it needs to reproduce the material properties as closely as possible, it should be able to predict some properties that it has not been fitted and it should be efficient.

Due to efficiency reasons higher terms than V_3, in Eq. (5.9), are often neglected. In order to simulate strongly bonded systems (with the absence of external forces) one needs to include the pair interaction V_2 and the three-body term V_3.

Two major classes of many-body potentials can be distinguished: bond-order potentials (BOP) and the embedded atom model (EAM).

The Tersoff potential is one of the potentials belonging to the BOP class. It has a three-body potential functional form which explicitly includes an angular contribution of the force called bond order – the strength of each bond depends on the local environment and is lowered when the number of neighbours is relatively high. The Tersoff potential can be written as the sum of the attractive f_A and repulsive f_R pair potentials:

$$V_{ij} = f_C(r_{ij})[f_R(r_{ij}) + b_{ij} f_A(r_{ij})], \tag{5.10}$$

where r_{ij} is a distance between the atoms, b_{ij} is the bond-order term and f_C is a smooth cut-off function.

The Environment-Dependent Interatomic Potential (EDIP) [28] is also classified as being BOP and is an efficient and realistic model for interatomic forces in covalent materials [29, 30]. It consists of the two-body and three-body terms that both depend on the local environment of atom through the effective coordination number.

The embedded atom method (EAM) [31, 32] is an interatomic potential that treats the material as nuclei embedded in a charged density distribution ('electron sea'). This approach represents the total energy of the system as two additive terms, a pairwise sum of interactions between atoms, and a term representing the electron density of each atomic site:

$$E = \sum_i F_i(\sum_{i \neq j} \rho_j(r_{ij})) + \frac{1}{2} \sum_{i,i \neq j} V_{ij}(r_{ij}), \tag{5.11}$$

where E is the total energy of the system, i and j indicate the unique pairs of atoms within the N atoms of the system, r_{ij} is their interatomic separation, $V(r_{ij})$ is a pairwise potential, and $F(\rho_j)$ is the embedding function for atom j which depends on the electron density ρ_j, experienced by that atom. Due to their analytical formalism, EAM type potentials describe metallic systems exceptionally well and are computationally very efficient.

5.2 Binary Collision Approximation

Binary collision approximation (BCA) simulation method is a useful tool for studying high energy cascades [33, 34]. This method approximates the full atomic dynamics of a material by a series of binary collisions neglecting possible many body effects. When an energetic atom enters the material it collides with the target atoms. The scattering angle and the energy transferred to the target atom can be obtained by solving the classical scattering integral for each collision, Eq. (4.3). The impact parameter b and the azimuthal angle ϕ (the angle from the initial direction of a particle) are chosen randomly for each collision. The impact parameter is selected within the scattering cross section ($d\sigma = 2\pi b db$) and is dependent on the composition and the atomic density of the target material.

The BCA is a computationally very efficient simulation method due to the fact that it considers only atoms that have energy above a chosen cut-off value. If the kinetic energy falls below this cut-off value, the atom is treated as stationary and its movement is not further considered. A criterion for atom being stationary can be accounted for using a cut-off energy. In Publication **IV** the cut-off energy for the bulk and surface layer is chosen to be 3 eV and 1 eV, respectively. In the BCA code CASWIN [35], used in this thesis, a particle is treated as sputtered if its energy in the direction perpendicular to the surface has exceeded the surface binding energy. The determination of the damage production in BCA simulations strongly relies on the threshold displacement energy (E_d), which is the parameter describing the energy needed to permanently displace an atom from its position.

The interatomic potential between two particles in the BCA simulation is given by a screened Coulomb's potential:

$$V(r) = \frac{1}{4\pi\epsilon_0} \cdot \frac{Z_1 \cdot Z_2 \cdot e^2}{r} \cdot \phi(r/a), \tag{5.12}$$

where e is the electron charge, ϵ_0 is the permittivity of a vacuum, Z_1 and Z_2 are the charges of the interacting nuclei, r the distance between them, a is the so-called screening parameter.

The potential $V(r)$ in Eq. (5.12) becomes purely Coulombic at short distances. At larger distances the Coulomb potential is screened by the surrounding electrons, and the effect of the electrons can be described by introducing a dimensionless screening function $\phi(r/a)$ to the Coulomb potential. A very commonly used repulsive potential is the one given by Ziegler, Biersack and Littmark [17], suggesting that the universal screening potential is a function of the dimensionless reduced radius x which is related to the real radius by the scaling length a_U, and depends on the charges of the involved atoms:

$$x = \frac{r}{a_U}, \tag{5.13}$$

and

$$a = a_U = 0.8854 \cdot \frac{a_0}{Z_1^{0.23} + Z_2^{0.23}}, \tag{5.14}$$

where $a_0 = 0.529$ Å is the Bohr radius. The resulting in screening function $\phi(x)$ is:

$$\phi(x) = 0.1818e^{-3.2x} + 0.5099e^{-0.9423x} + 0.2802e^{-0.4029x} + 0.02817e^{-0.2106x} \tag{5.15}$$

This is the so-called ZBL repulsive potential.

In Publication **IV** the BCA simulation method is used to simulate single ion impacts to study the displacements and sputtering of the target atoms.

Chapter 6

Results

6.1 Impurity Induced Defect Formation

As described previously in Chapter 3, defects such as monovacancies are always present in the materials above the absolute zero. Similarly, all solids in nature contain a certain amount of impurities. The presence of foreign atoms may greatly affect material properties.

Over the past couple of decades H – metal interaction has been of a great interest, since the experimental observations of H assisted vacacy formation [9, 10]. Typically near the melting point of metals the equilibrium vacancy fractions range from about 10^{-4} to 10^{-3} while due to the presence of large amounts of H this fraction can increase up to 0.1 – 0.3. The origin of this phenomenon, often referred to as the superabundant vacancy (SAV) formation, lies in the lowering of the total free energy of the system due to the H trapping in vacancies.

As a part of this thesis, a theoretical thermodynamics model was developed to quantitatively demonstrate the vacancy formation as a function of temperature and the impurity concentration.

In Publication **I**, the total equilibrium vacancy fraction is calculated as a function of H fraction in four metals: palladium (Pd), nickel (Ni), cobalt (Co) and iron (Fe). The results from the theoretical thermodynamics calculations are compared with the experimental data by Fukai and co-workers, where the authors using the lattice contraction measurements for Ni, Co, Pd and X-ray diffraction measurements for Fe, observed SAV formation [36, 37]. The energy and entropy parameters for vacancy formation and H binding to the vacancies are found from the literature and used as the input for our theoretical thermodynamics model. The H fractions and temperature of the system are taken from the corresponding experiments [36, 37].

The total vacancy fraction in a material can be expressed as the sum of fractions of monovacancy, divacancy and larger vacancy clusters:

$$[V_{tot}] = [V_1] + 2\,[V_2] + 3\,[V_3] + ... \tag{6.1}$$

Several thermodynamics approaches may be employed to estimate the total vacancy concentration in materials. The simplest way is to take into account only monovacancy thermodynamics neglecting larger vacancy clusters completely. This is a sufficient approach when divacancies and larger vacancy clusters give a negligible contribution to the total vacancy fraction, e.g, in the case of a pure metal with a large divacancy formation energy. However, when the monovacancy fraction is large, vacancy clustering takes place. Besides, when the divacancy formation energy is relatively small, the divacancy contribution to the total vacancy fraction can not be neglected. The efficient way to estimate the divacancy fraction $[V_2]$ is to calculate it from the monovacancy fraction and taking into account their binding properties [38]:

$$[V_2] = \frac{z}{2} \exp\left(\frac{\Delta S_b^{v_2}}{k_B}\right) [V_1]^2 \exp\left(\frac{-E_b^{v_2}}{k_B T}\right), \tag{6.2}$$

where z is the configurational factor that accounts for possible orientations of the divacancy, $E_b^{v_2}$ is the divacancy binding energy, $\Delta S_b^{v_2}$ is the divacancy binding entropy and for simplicity the entropy term $\exp\left(\frac{\Delta S_b^{v_2}}{k_B}\right)$ is assumed to be unity. This commonly used assumption is accurate for divacancy estimation in pure metals. In the presence of H Eq. 6.2 largely overestimates the divacancy fraction and, therefore, should not be used when studying SAV formation.

In this thesis, a more accurate way to study SAV's is proposed: the thermodynamics of monovacancy and divacancy formation is considered, the binding energy of each trapped H is taken into account and the defect entropy terms are included, as described in Publication **I**.

The comparison of the two approaches is shown in Fig. 6.1, the thermodynamics of only monovacancies with divacancies being calculated from the squared monovacancy fraction, as in Eqs. (6.1, 6.2), and the thermodynamics of both – monovacancy and divacancy formation, shown in Eqs. (3.22 – 3.25). The results show that at high H fractions, the vacancy fraction is overestimated if the divacancy fraction is assumed to be proportional to the monovacancy fraction squared. Besides, the total vacancy fraction becomes increasingly overestimated for metals with larger divacancy binding energies.

In Fig. 6.2, a comparison of equilibrium vacancy fraction in Ni–H system is presented, calculated using the thermodynamics model of monovacancies and divacancies, as in Eqs. (3.22 – 3.25), and

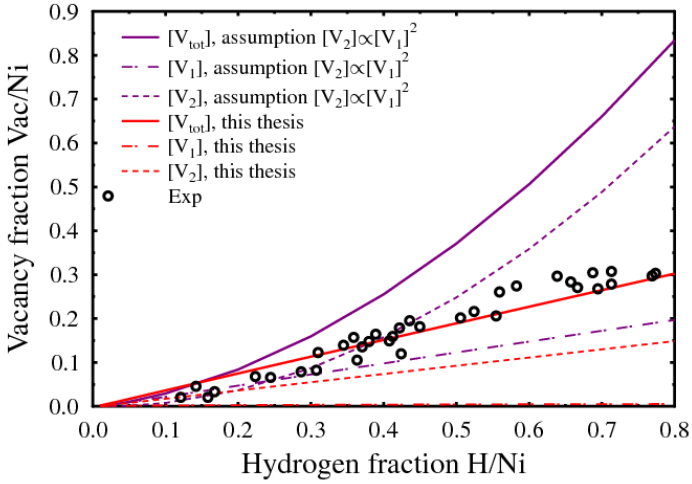

Figure 6.1: Comparison between theoretically calculated vacancy fraction as a function of H fraction for the Ni-H system using thermodynamics model taking into account the monovacancy and divacancy thermodynamics as shown in Eqs. (3.22 – 3.25), and taking into account only monovacancy thermodynamics and obtaining divacancies from Eqs. (6.2, 6.1), both methods are presented and discussed in detail in Publication **I**. The parameters used in the thermodynamics calculations are: $E_f^{v_1} = 1.37$ eV, $E_f^{v_2} = 2.42$ eV, $\Delta S_{vib}^{v_1} = 2.00\ k_B$, $\Delta S_{vib}^{imp1} = -0.1\ k_B$, T = 1100 K. The fitting constant to the H cumulative binding energy to monovacancy and divacancy: A = 0.005273, B = −0.070655, C = 0.640694, D = 0.002492, E = −0.061665, F = 0.828168.

the thermodynamics of only monovacancies Eqs. (3.20) (completely neglecting the presence of divacancies). A very good agreement is found for low H fractions. However, at larger H fractions, where the divacancy fraction becomes increasingly dominant over the monovacancy fraction, a deviation is observed between both approaches. This stems from the higher H binding energy to the divacancy. As a consequence the thermodynamics of only monovacancies is capable to accurately describe the total equilibrium vacancy fraction below the H fraction $\sim 10^{-3}$. Above this H fraction (if H is stronger bound to the divacancy than to the monovacancy), the divacancy contribution becomes dominant and the thermodynamics of both monovacancies and divacancies is a more accurate way to calculate the total equilibrium vacancy fraction.

To prove the proposed hypothesis, the case where H does not bind to vacancies is demonstrated (the binding energy of 0 eV is assumed). The temperature of the system is chosen to be the melting point of pure Ni. In Figure 6.3, as anticipated, the monovacancy contribution to the total equilibrium vacancy fraction dominates over the divacancy contribution. Interestingly,

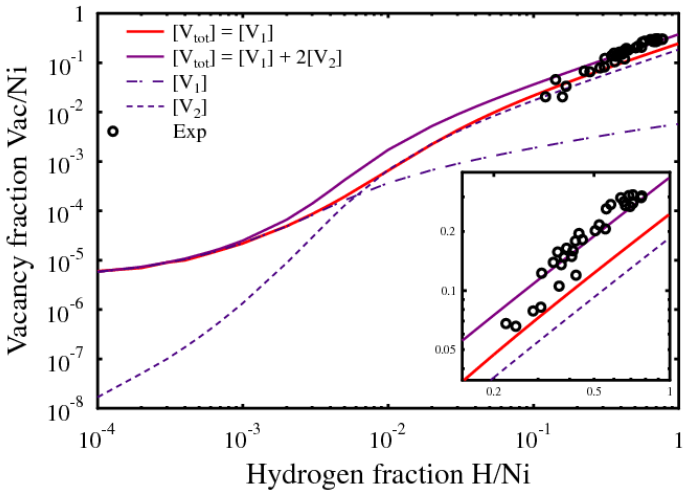

Figure 6.2: Comparison between theoretically calculated vacancy fraction as a function of H fraction for the Ni-H system using the thermodynamics model of monovacancies and divacancies Eqs. (3.22 - 3.25), and the thermodynamics of only monovacancies Eq. (3.20), from Publication **I**. In the inset, we show that the thermodynamics for only monovacancies is not sufficient to accurately describe the total vacancy fraction. Note the logarithmic scale. The parameters used in the thermodynamics calculations are the same as in Fig. 6.1.

even if the H binding energy to vacancies is zero, SAV formation is observed at H fractions above 10%. The reason for SAV formation at large H fractions is the H configurational entropy: when a vacancy is formed, more possible sites to accommodate H become available, increasing the total entropy.

This leads to the other important conclusion that H configurational entropy is one of the reasons for the SAV formation observed most often in an FCC phase. Depending on the host material, in an FCC structure H can occupy one octahedral or two tetrahedral interstitial sites per host atom, whereas in a BCC crystal H can be distributed over six tetrahedral or three octahedral interstitial positions per host atom. As a consequence, the formation of a vacancy in an FCC metal gives rise to more configurations to distribute H than in the BCC metal.

To show the effect of the material structure on SAV formation, in Fig. 6.4 a hypothetical metal is presented (the parameters used in the thermodynamics calculations $E_f^{v_1} = 1.50$ eV, $E_f^{v_2} = 2.99$ eV, $\Delta S_{vib}^{v_1} = 2.00\ k_B$, $\Delta S_{vib}^{imp1} = -0.1\ k_B$, T = 1100 K) with two different structures – BCC and FCC. The hypothetical metal is assumed to accommodate H in six tetrahedral interstitial

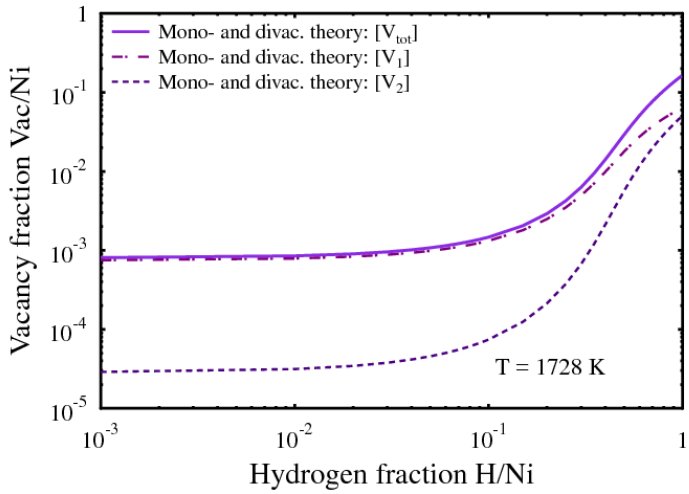

Figure 6.3: The vacancy fraction as a function of H fraction for the Ni-H system using the thermodynamics approach as in Eqs. (3.22 – 3.25), from Publication **I** (the parameters used in the thermodynamics calculations $E_f^{v_1} = 1.37$ eV, $E_f^{v_2} = 2.42$ eV, $\Delta S_{vib}^{v_1} = 2.00\ k_B$, $\Delta S_{vib}^{imp1} = -0.1\ k_B$, T = 1728 K). Here the binding parameters A, B, C and E, F, G for monovacancies and divacancies, respectively, are zero. Note that even if the H binding energy to vacancies is zero, the vacancy fraction increases due to the presence of H.

positions (m = 6) in BCC phase and one octahedral interstitial position, when it is in the FCC phase (m = 1). The figure shows that a metal with the FCC structure has about a two decade larger vacancy fraction than a metal with the BCC structure, with the same energy and entropy parameters.

To conclude the main results of this chapter: the thermodynamics of only monovacancies is capable to accurately describe the total equilibrium vacancy fraction below the H fraction 10^{-3}. Above this H fraction (if H is stronger bound to the divacancy than to the monovacancy), the divacancy contribution becomes dominant and the thermodynamics of both monovacancies and divacancies is a much more accurate way to calculate the total equilibrium vacancy fraction. Obtaining the divacancy fraction from the monovacancy fraction squares highly overestimates the total vacancy fraction and is not suitable for studying SAVs at large H fractions. One of the factors strongly mediating SAV formation is the H configurational entropy. It is responsible for vacancy formation at large H fractions even if there is no binding between the H and a vacancy, and is a reason for SAVs being seen mainly in FCC metals.

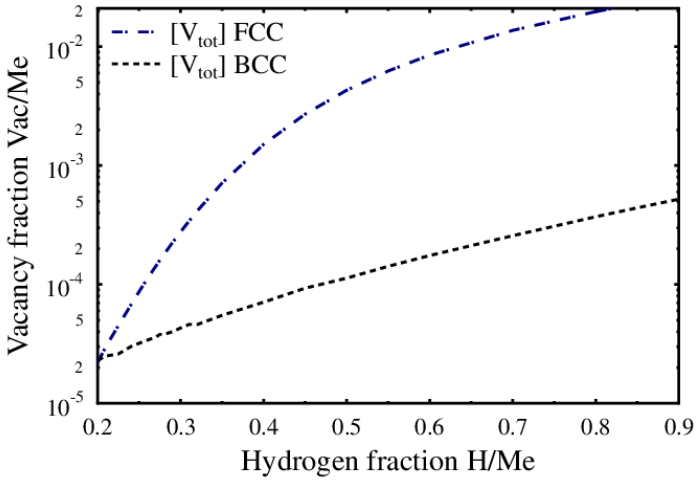

Figure 6.4: The equilibrium vacancy fraction as a function of H fraction for a hypothetical metal with FCC and BCC structure, note the logarithmic y scale. The difference between the two structures arises due to the H configurational entropy factor (Publication **I**).

6.2 Defect Dynamics

6.2.1 Diffusion

In Publications **II** and **III** the diffusion of monovacancies and H impurities in tungsten is studied employing the MD method. The diffusing particle is tracked during simulation and the diffusion coefficient is determined by the improved Einstein-Smoluchowsky equation with the independent interval method (IIM) [39], as follows:

$$D = \frac{1}{N} \frac{\sum_{i}^{N} R_i^2(t)}{6 \sum_{i}^{N} \Delta t_i}, \tag{6.3}$$

$R_i^2(t)$ being the squared displacement of the diffusing species, Δt is the diffusion time and N is the number of intervals the diffusion path is divided into.

Monovacancy diffusion

Table 6.1: Melting temperatures, diffusion activation energies E_a, pre-exponential factors D_0 and attempt frequencies for W ν.

Method	T_m(K)	E_a (eV)	D_0 (m^2/s)	ν (Hz)
Exp [16, 40]	3695	1.8	$4.0\times10^{-6*}$	-
DFT [42, 43]	–	1.71, 1.78	-	-
BOP-1 [44]	2750	1.84	1.5×10^{-5}	1.2×10^{15}
BOP-2 [42]	4550	1.59	4.0×10^{-6}	3.2×10^{14}
BOP-3 [45]	4550	1.69	4.2×10^{-6}	3.4×10^{14}
EAM [46]	$\sim$ 3750	2.09	1.0×10^{-5}	8.2×10^{14}

*Data extracted from self-diffusion experiments

In Publication **II**, employing the MD simulation method and using four interatomic potentials (three bond order potentials: BOP-1, BOP-2 and BOP-3 and an EAM potential) the diffusion of a single vacancy is simulated over a wide temperature range.

By fitting the Arrhenius function to the diffusion coefficients attained from the simulations, the diffusion parameters such as monovacancy migration energy and the diffusion pre-exponential factor are obtained. The experimental and simulated melting points and diffusion parameters are summarized in Table 6.1.

The monovacancy migration energies are found to be in the range from 1.59 to 2.09 eV, depending on the interatomic potential. This is in reasonable agreement with the experimental value 1.78 eV [40].

The diffusion pre-exponential factor for monovacancy diffusion is found to be two to three orders of magnitude higher than commonly used in computational studies [41], resulting in the highest attempt frequency (for BOP-1) of the order of 10^{15} Hz. This high jump frequency is quite unexpected, considering that a vacancy jump in BCC metals occurs when any of the eight one nearest neighbour (1NN) W atoms with an approximated jump frequency of 5×10^{12} Hz jumps into the vacancy.

When analyzing the vacancy diffusion process in more detail, multiple monovacancy jumps have been discovered: at higher temperatures (above about 2/3 of the melting temperature T_m) an increasing number of the vacancy position changes are not 1NN jumps, but two or three atoms in the $\langle 111 \rangle$ row move towards the empty lattice position, i.e. the vacancy moves two or three nearest neighbour distances at once.

Furthermore, it is shown that a simultaneous movement of W atoms occurs not only along the $\langle 111 \rangle$ direction: a significant number of two nearest neighbour jumps of monovacancy occur first in $\langle 111 \rangle$ direction, then in either $\left[1\,\bar{1}\,\bar{1}\right]$, $\left[\bar{1}\,1\,\bar{1}\right]$, $\left[\bar{1}\,\bar{1}\,1\right]$, giving the total displacement of

≈ 3.17 Å, later referred to as L_A, or in $[11\bar{1}]$, $[1\bar{1}\,1]$, $[\bar{1}\,11]$ direction, with total displacement ≈ 4.48 Å referred to as L_B. The nearest and next-nearest neighbour jumps are illustrated in Fig. 6.5.

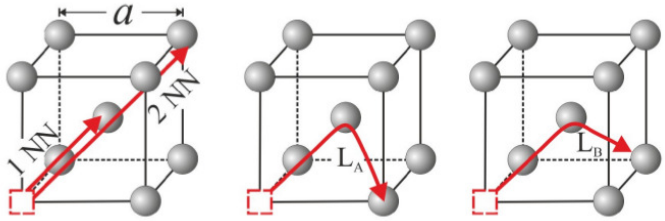

Figure 6.5: Monovacancy jump paths in BCC metals.

The sum of all these jump contributions (1NN jumps, as well as the other diffusion mechanisms), explain the exceptionally high effective monovacancy jump frequency obtained from the MD simulations.

The probabilities for different nearest neighbour jumps for a single vacancy in W was calculated from the MD simulations, and it was found that already at 2/3 of T_m, a significant number of vacancy jumps are larger than the 1NN jump, which gives an evident contribution to the diffusion coefficient with different activation parameters.

The total diffusion coefficient D_{tot}, taking into account all diffusion mechanisms, may be written:

$$\begin{aligned} D_{tot} &= D_1 \cdot \exp\left(\frac{-E_1}{k_B T}\right) + D_2 \cdot \exp\left(\frac{-E_2}{k_B T}\right) + D_3 \cdot \exp\left(\frac{-E_3}{k_B T}\right) + \\ &\quad + D_A \cdot \exp\left(\frac{-E_A}{k_B T}\right) + D_B \cdot \exp\left(\frac{-E_B}{k_B T}\right), \end{aligned} \tag{6.4}$$

where D_i and E_i are pre-exponential factors and migration barriers, respectively, for i=1: 1NN jumps, i=2: 2NN, i=3: 3NN jumps, i=A: L_A jumps and i=B: L_B jumps.

The W monovacancy diffusion coefficients obtained with MD and the fit to the Arhenius function is shown in Fig. 6.6. The monovacancy diffusion exhibits the super-exponential behaviour. The multiple vacancy jumps could be one of the reasons for the upward curvature of the Arrhenius diagram and could possibly explain the increase in the diffusion coefficient above 2/3 T_m in the early W self-diffusion experiments [16].

Other mechanisms have also been proposed to interpret the slight upward curvature of the Arrhenius diagram, such as the simultaneous diffusion of monovacancies and larger vacancy

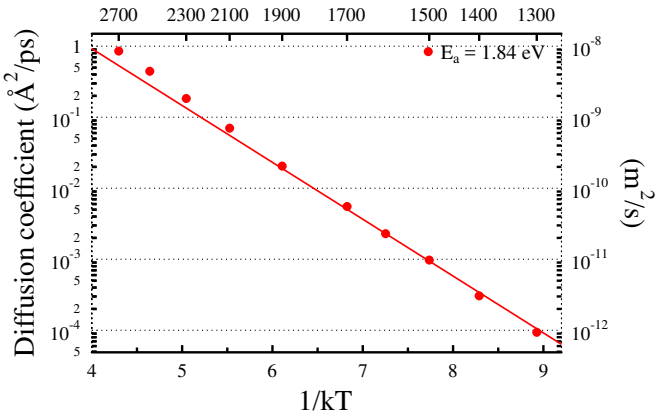

Figure 6.6: Arrhenius diagram for W monovacancy diffusion (BOP-1). Fitted $D_0 = 1.5{\times}10^{-5}$ m^2/s, $E_a = 1.84$ eV for temperatures 1300K – 1600K, resulting in the attempt frequency $\nu = 1.2 \times 10^{15}$ Hz. The diffusion coefficient shows the upward curvature of Arrhenius diagram at higher temperatures (Publication **II**).

clusters (divacancies), self-interstitial atom (SIA) diffusion, and the temperature dependence of vacancy formation and diffusion parameters.

Due to the fact that the binding energy for two W monovacancies, obtained by DFT and MD (Publication **II**), is close to 0 eV, the divacancy contribution is expected to play a minor role in the increase of self-diffusion coefficient. The formation energy of an SIA in W is over 9 eV [47, 48] making its thermodynamic contribution to self-diffusion negligible at any temperature. However, DFT studies show that the vacancy formation energy in W decreases somewhat at higher temperatures, which explains partly, nevertheless not fully, the deviation from Arrhenius behaviour [49].

Hydrogen diffusion

In Publication **III**, the diffusivity of H is studied using MD simulations over the temperature range from 300 K to 2000 K. At lower temperatures than about 200 K the quantum diffusion of H takes place which cannot be described by the classical MD. Therefore, temperatures below room temperature are not considered in this thesis. The H atom is an endothermic impurity in W with high solution energy E_{sol} of about 1 eV [50] leading to low equilibrium concentrations of H in W. However, large H flux from a fusion device, plasma source or ion implanter can result in concentrations that considerably exceed the equilibrium value in W. This H concentration is proportional to the incoming flux and inversely proportional to the H diffusivity.

The migration barrier for H in tungsten is obtained from an Arrhenius fit to MD simulated diffusion coefficients to be 0.25 eV. This value is in agreement with the DFT value 0.26 eV [47]. However, the commonly accepted and recommended value for the H migration barrier from Fraunfelder experiments [50] is 0.39 eV, which is significantly larger.

The Arrhenius diagram for simulated and experimental H diffusion coefficients is shown in Fig. 6.7. The MD simulation results agree with the Fraunfelder data when the low temperature points are omitted from the fit (see Fig. 6.7, red line). This omission is justified due to the H trapping effects [51]: at low temperatures when H is occasionally trapped into other defects such as vacancies, the effective diffusion coefficient becomes lower than the actual diffusion coefficient resulting in the overestimated activation energy for H diffusion. Due to this fact the value of 0.25 eV for H migration barrier in W should be used in the calculations instead of the 0.39 eV commonly used.

To obtain the impurity diffusion coefficient from MD simulations the Eq. (6.3) can be used. However, the distance squared in Eq. (6.3) includes also the random oscillation of the H atom around its equilibrium position. This means that when a large number of MD simulations are done, the obtained mean displacement squared is larger than the actual distance squared between two atomic equilibrium positions:

$$\left\langle \Delta R_{MD}^2 \right\rangle > \left\langle \Delta R^2 \right\rangle \tag{6.5}$$

where $\langle \Delta R_{MD}^2 \rangle$ is the simulated mean displacement squared including random oscillation, and $\langle \Delta R^2 \rangle$ is the mean displacement squared (distance squared between two atomic equilibrium positions).

This discrepancy gets even more significant when the diffusion path is divided into large number of intervals N (in order to improve statistics). For increasing number of intervals the random oscillation around the equilibrium position becomes comparable to the diffusion path itself, increasing the error for the calculated diffusion coefficient.

In Publication **III**, a new method to obtain the correct diffusion coefficient is developed:

$$D = \frac{\sum_i^N \Delta R_{MD,i}^2 - N \times 2 \left\langle \Delta r^2 \right\rangle}{6 \sum_i^N \Delta T_i}, \tag{6.6}$$

where $\Delta R_{MD,i}^2$ is the simulated displacement squared and $\langle \Delta r^2 \rangle$ is the mean oscillation distance squared around the atomic equilibrium position. The $\langle \Delta r^2 \rangle$ is obtained from the simulations averaging over thousands of MD simulated position points.

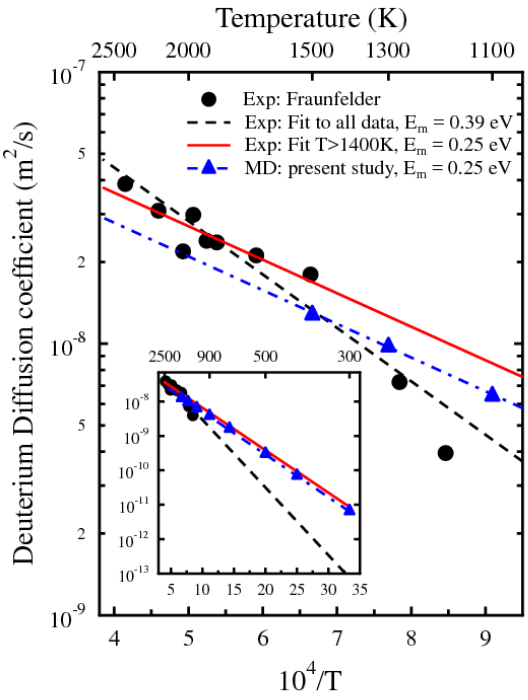

Figure 6.7: Arrhenius plot of simulated and experimental H isotope (deuterium) diffusion coefficients. The Fraunfelder data has been divided by the square root of two to obtain the correct values for deuterium. The red line is the fit to the Fraunfelder data where the two lowest temperature points, T < 1400 K, have been omitted. The labels and units in the inset are the same as for the main plot.

By using Eq. (6.6), the diffusion path can be divided into many intervals (to improve statistics) and still an accurate diffusion coefficient can be obtained.

In Publication **III**, it is shown that the H diffusion has a strong dependence on its concentration: the diffusivity of H decreases with the increasing concentration. At high H concentration, the lowering of the diffusion coefficient can be mostly attributed to the neighbouring interstitial site blocking.

On the other hand, the diffusion of H atoms is significantly affected by H cencentration already at H concentrations above 1%. The observed diffusivity decrease can be explained by the close range repulsive H-H interaction [52], where it was seen by Liu et al. [53] that the H atoms repel each other for distances below about 3.2 Å.

This rather long range repulsion prevents a H atom from diffusing towards another H atom, decreasing the effective diffusion coefficient. This explanation seems feasible, as the observed diffusion coefficient reduction is largest at low temperatures where a small repulsion between atoms is enough to keep them apart. The equation accounting for the concentration dependent H diffusion is proposed to be:

$$D = D_0 \exp\left(-\frac{(X-\alpha)^2}{\beta}\right) \exp\left(-\frac{(E_m + \gamma X^\delta)}{k_B T}\right), \tag{6.7}$$

where X is the number of H atoms divided by the total number of interstitial sites: $X = \frac{H}{W \cdot 6}$, the BCC lattice has six TIS per atom. Parameters D_0, E_m, α, β, γ and δ are the fitting parameters. The lines in Fig. 6.8 show that Eq. (6.7) describes very well the simulated diffusion coefficients for the whole H/W ratio as well as the temperature region. The fitted parameter values are: $D_0 = 1.2737{\times}10^{-7}$ m^{2}s^{-1}, $E_m = 0.2430$ eV, $\alpha = 0.028314$, $\beta = 0.002167$, $\gamma = 2.13773$ and $\delta = 0.73842$. The decreasing H diffusion coefficient as a function of H concentration might have

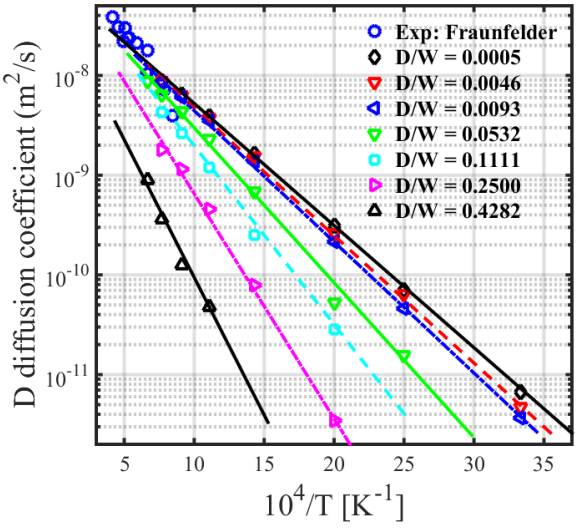

Figure 6.8: The simulated H isotope (deuterium) diffusion coefficients as a function of temperature and H/W fraction. The Fraunfelder data (circles) has been divided by the square root of deuterium's atomic mass (publication **II**). The solid lines are given by Eq. (6.7).

serious implications on the properties of tungsten material in H-rich environments. In high H flux experiments, the concentration of H in W might become much higher than expected due to the self-induced decrease in the diffusivity.

This is especially important at lower temperatures as seen in Fig. 6.8, where the diffusivity reduction as a function of concentration is most pronounced.

6.2.2 Displacements

Ion irradiation is a tool to study and alter material properties. It is a widely used approach to introduce impurity atoms in semiconductor materials and to study the irradiation tolerance of shielding materials exposed to the particle bombardment. Ion-beam irradiation has proven to be a promising method for surface morphology modifications. Under certain conditions, ion irradiation can cause ripple formation on the target material surfaces. This phenomenon has been seen on various semiconductor [54] and metal surfaces [55, 56] and has been intensively studied for the past couple of decades.

A recent theoretical model based on the displacement analysis obtained from the MD simulations of single ion impacts suggests that the ripple formation is dominated by the atom redistribution in a target, the sputtering being irrelevant [57]. The theoretical approach to predict the surface pattern formation requires knowledge of the "crater function" - the partial differential equation describing the evolution of the surface. The most direct method of determining the crater function is molecular dynamics (MD) studies of individual ion impacts. The MD technique based on the analytical interatomic potentials is limited in the size of the system it can model, however, at high ion energies the size of the simulation cell must be large enough to enclose the evolving cascade. This creates a demand for a computationally more efficient method - BCA.

In Publication **IV**, the single 1 keV Ar^+ ion impacts on amorphous silicon (a-Si), crystalline Si and W have been simulated with MD and BCA techniques. The average displacement profiles have been calculated and compared for the two fundamentally different computational methods (Fig. 6.9, 6.10 and 6.11). The results reveal a significant shortcoming of the BCA approach when applied to materials that are amorphous or become amorphous during ion irradiation. The study shows that at displacements above about 5 Å, the MD and BCA displacement distributions are in a good agreement for all three target materials. At small displacements – below about one bond length – the BCA and MD results show large discrepancies for a-Si and crystalline Si, and gives good agreement for W. This difference between MD and BCA simulations arises due to the neglect of many-body interactions in BCA. The BCA approach misses a very large number of small displacements seen in MD and attributed to the collective phenomenon of amorphous material flow. This shortcoming could seriously compromise the ability to use BCA to accurately evaluate crater functions for description of surface pattern formation. Interestingly, the BCA

method, which does not account for the crystal structure of a material in any way, describes the atom displacements clearly better for crystalline than amorphous materials. Tungsten does not become amorphized upon irradiation and, therefore, the BCA and MD results are in good agreement.

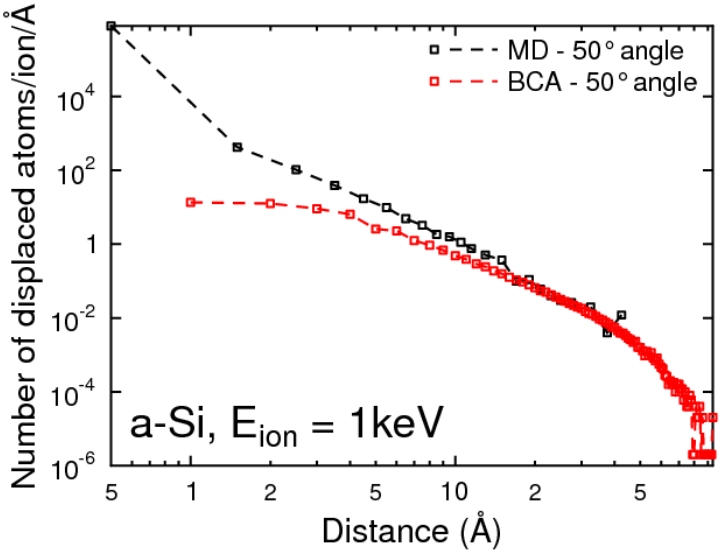

Figure 6.9: Atom displacement statistics for single 1 keV Ar^+ impact on amorphous Si at 50^o incidence angle. Comparison between the MD and BCA methods, from Publication **IV**.

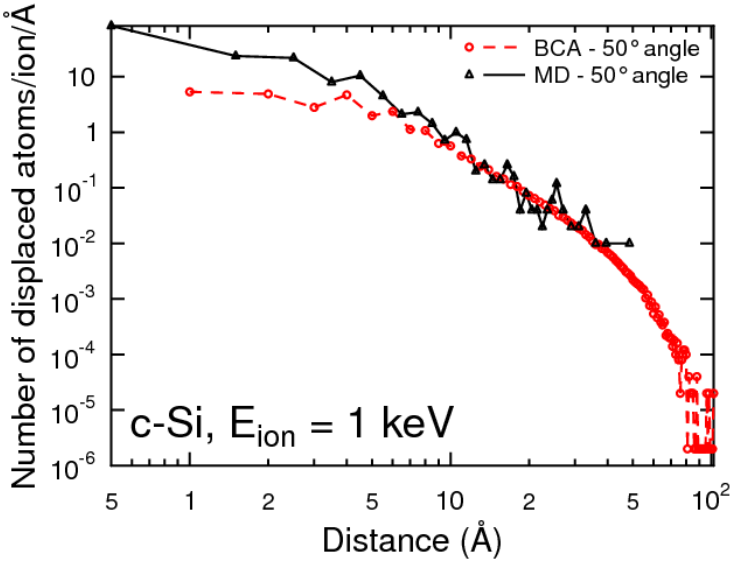

Figure 6.10: Atom displacement statistics for single 1 keV Ar^+ impact on crystalline Si at 50^o incidence angle. Comparison between the MD and BCA methods, from Publication **IV**.

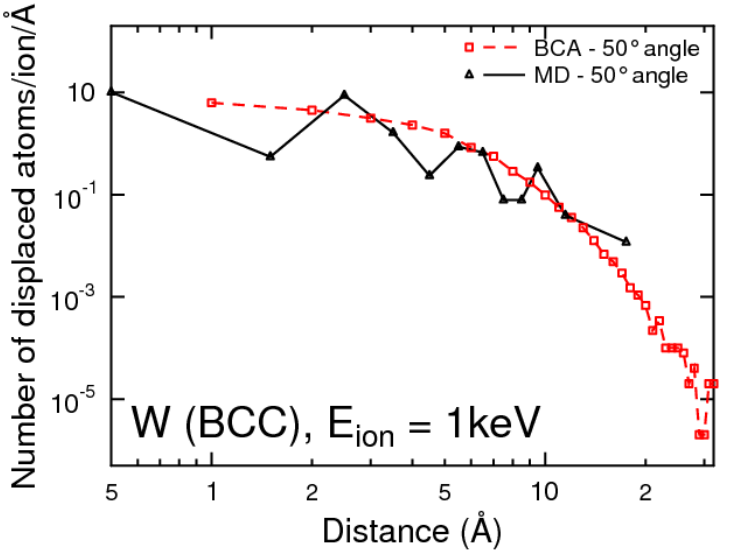

Figure 6.11: Atom displacement statistics for single 1 keV Ar^+ impact on crystalline W at 50^o incidence angle. Comparison between the MD and BCA methods, from Publication **IV**.

Chapter 7

Summary

The purpose of this thesis is to deepen knowledge of defect formation and diffusion phenomena. In this thesis the defect formation in metals is studied applying thermodynamic theory. A general thermodynamics model, developed by the author, quantitatively demonstrates vacancy formation as a function of temperature and impurity concentration. For the correct description of the free energy of the system, the binding energies of each trapped impurity, the vibrational entropy of defects and the thermodynamics of divacancy formation are taken into account. The results of the thermodynamics calculations are compared with the available experiments and are found to be in good agreement. The model shows that the divacancy fraction makes a major contribution to the total equilibrium vacancy fraction due to the higher impurity binding energy to divacancies than to monovacancies. The results also indicate that calculating the thermodynamic formation of only monovacancies is not a sufficient approach for estimating the total equilibrium vacancy fraction in most metals. The comparative study between different thermodynamics approaches and experiments shows that the divacancy contribution must be calculated according to the thermodynamics by minimizing Gibbs free energy, and demonstrates that the approximation of the divacancies being proportional to the squared monovacancy fraction can be used only for pure metals or metals containing small amounts of impurity atoms, making it an unsuitable approach for calculating superabundant vacancy formation.

The thermodynamics model also shows that vacancies are formed in metals due to the presence of impurities such as H, and at high impurity fraction vacancies are formed regardless of the impurity binding energy to the vacancy. The reason for this phenomenon is shown to be the impurity configurational entropy increase upon the vacancy formation which explains superabundant vacancy formation being more pronounced in the FCC phase than in the BCC phase.

Inspired by fusion research the diffusion of monovacancies and H impurities in tungsten has been studied employing the MD technique. The hydrogen migration barrier is revised and proposed to be 0.25 eV. A new general method is derived to obtain an accurate diffusion coefficient in simulations dealing with the random oscillations of diffusing species around the equilibrium position. This correction improves the accuracy of determining the diffusion coefficient at all temperatures, but the main advantage is that it makes it possible to simulate atomic diffusion, and determine the corresponding diffusion coefficients at lower temperatures than previously. The H diffusion is shown to be concentration dependent due to the neighbouring site blocking at high concentrations and repulsive H interactions.

The monovacancy diffusion was studied in tungsten, and it was found that the diffusion coefficient exhibits a slight increase at high temperatures. The reason for this upward curvature is not fully established yet. The molecular dynamics simulations indicate the occurrence of multiple nearest neighbour vacancy jumps that take place mostly at temperatures of 2/3 of the melting point. Moreover, the diffusion pre-exponential factor was calculated for monovacancy diffusion in tungsten and found to be higher than expected resulting in a monovacancy diffusion attempt frequency two to three orders of magnitude higher, of about 10^{15}, than commonly used in computational models.

Lastly, a single Ar ion bombardment of amorphous Si, crystalline Si and BCC tungsten was studied. The results for molecular dynamics and binary collision methods are compared to answer a question of the suitability of BCA for studying atomic displacements when it comes to explaining such phenomena as the formation of ripples. The results from both methods show good agreement for crystalline materials, however, large discrepancies are observed at distances below about one bond length for amorphous materials or materials that become amorphous during irradiation. Due to the nature of the BCA simulations that neglect many-body interactions, it is impossible to reproduce the very large amount of small displacements present in MD. This shortcoming of BCA could seriously compromise the ability to use BCA to describe the amorphous material flow which hes been reported to be the main reason for ripple formation. Interestingly, the Monte Carlo BCA simulations, which do not account for the crystal structure of a material in any way, describe the atom displacements clearly better for crystalline than amorphous materials.

The results of this thesis contribute to a better understanding of defect formation and diffusion in metals. However, predicting the material performance in such extreme conditions as in fusion reactors is very complex and needs extensive studies. Vacancy formation in tungsten should be studied as a function of impurity flux and fluence in future studies. For this purpose the thermodynamics model can be combined with the Kinetic Monte Carlo simulations or the mean

field rate equation theory. Such an approach together with the experimental studies would allow us estimate the vacancy formation in material and impurity retention as a function of incoming impurity amounts. Although ion induced nano-patern formation have been studied for decades, the complete understanding of processes taking place in materials under different conditions is still lacking. Future work in this field should include examining the the role of the stress accumulation in the amorphous layer during the irradiation process.

Acknowledgements

I would like to thank the former and the current head of the Department of Physics at the University of Helsinki, Prof. Juhani Keinonen and Prof. Hannu Koskinen, as well as the head of the Accelerator Laboratory Prof. Jyrki Räisänen for providing the facilities for doing the studies presented in this thesis. I extend my thanks to Prof. Jyrki Räisänen for giving me directions that have helped me to prepare for the defense of this thesis. I am most indebted to Prof. Kai Nordlund for giving me the opportunity and welcoming me to his research group. I thank Prof. Kai Nordlund for believing in me and a never ending positive attitude.

I am grateful to Doc. Fluyra Djurabekova and Dr. Marie Backman for supervising me during the first years at the Accelerator Laboratory.

I thank all my colleagues at the Accelerator Laboratory for relaxed discussions about nearly everything – being in such international work environment helped me to deal with several culture shocks experienced in Finland. I would like to give special thanks to Andrey for being a perfect colleague, thank you for being always so kind, patient and helpful. Thank you, Wei, for your friendship and for being such a positive and happy person. I would like to thank Alvaro for never refusing a helping hand and Fredi for always being there for me when I have needed. I am thankful to my former colleague Jussi for being my friend at the lab and outside of it, for being my person of trust and making my thesis better by proof-reading. I have been lucky to have such colleagues.

Most of all I want to thank my husband, my best friend and my biggest inspiration - Tommy. Your motivating attitude, thoroughness and enthusiasms made me realize the importance of our work and made it so much fun. I thank you for your patience, for supporting me through all the ”downs” and enjoying with me all the ”ups” this journey has had. Working with you has been an unforgettable experience. I also want to thank you for endless ideas for future work, that kept me focused and excited during these years. I would like to thank my daughter Amanda, for putting things in perspective and showing what is most important in life. I thank my mom, dad and my sister for supporting me and letting me travel away from home to pursue

my dreams. I thank my dear friends from Latvia - Laura, Pēteris and Liene with whom my friendship just got stronger during the years despite the distance. I thank you all for always waiting for and loving me.

Helsinki, 27th June 2017
Laura Bukonte

Bibliography

1. M. Eldrup, "Positron Methods for the Study of Defects in Bulk Materials", *Journal de Physique IV Colloque* 5, 95 (1995).

2. K. Tokunaga, T. Muroga, N. Yoshida, "Depth profile analyses of implanted deuterium in tungsten by secondary ion mass spectrometry", *Journal of Nuclear Materials* 220, 800, (1995).

3. T. Ahlgren, K. Heinola, E. Vainonen-Ahlgren, J. Likonen and J. Keinonen, "Quantification of deuterium irradiation induced defect concentrations in tungsten", *Nuclear Instruments and Methods in Physics Research B* 249, 436 (2006).

4. K. Heinola, T. Ahlgren, E. Vainonen-Ahlgren, J. Likonen and J. Keinonen, "Deuterium irradiation-induced defect concentrations in tungsten", *Physica Scripta* T128, 91 (2007).

5. F. Mandl, *Statistical Physics*, (John Wiley and Sons, Chichester, U.K., 1971).

6. K. L. Murty and I. Chari, *An Introduction to Nuclear Materials: Fundamentals and Applications*, (Wiley-VCH Verlag and Co., Weinheim, Germany, 2013).

7. F. A. Kröger, *The Chemistry of Imperfect Crystals*, (North-Holland, Amsterdam, and Wiley, New York, 1964).

8. M. F. Horstemeyer, *Integrated Computational Materials Engineering (ICME) for Metals*, (A John Wiler and Sons, New Jersey, 2012).

9. Y. Fukai and N. Okuma, "Evidence of copious vacancy formation in Ni and Pd under a high hydrogen pressure", *Japanese Journal of Applied Physics* 32, L1256, (1993).

10. Y. Fukai and N. Okuma, "Formation of superabundant vacancies in Pd hydride under high hydrogen pressures", *Physical Review Letters* 73, 1640 (1994).

11. H. Mehrer, *Diffusion in Solids: Fundamentals, Methods, Materials, Diffusion-Controlled Processes*, (Springer Series in Solid-State Sciences, Berlin, 2007).

12. G. Vineyard, "Frequency factors and isotope effects in solid state rate processes", *Journal of Physics and Chemistry of Solids* 3, 121 (1957).

13. F. Grandjean, G. J. Long, K. H. J. Buschow, *Interstitial Intermetallic Alloys*, (Kluwer Academic, Dordrecht, 1995).

14. R. J. Borg, G. J. Dienes, *An Introduction to Solid State Diffusion*, (Academic Press, London, 1988)

15. A. Einstein, "On the movement of small particles suspended in stationary liquids required by the molecular-kinetic theory of heat", (in German) Annalen der Physik 17, 549 (1905).

16. J. N. Mundy, S. J. Rothman, N. Q. Lam, H. A. Hoff and L. J. Nowicki, "Self-diffusion in tungsten", *Physical Review B* 18, 6566 (1978).

17. J. F. Ziegler, U. Littmark and J. P. Biersack, *The stopping and range of ions in solids*, (J.F. Ziegler, J.P. Biersack, U. Littmark. Pergamon New York, 1985).

18. M. Nastasi, J. W. Mayer, and Y. Wang, *Ion Beam Analysis. Fundamentals and Applications*, (CRC Press, Boca Raton, 2014).

19. H. H. Andersen, "The Depth Resolution of Sputter Profiling", *Applied Physics* 18, 131 (1979).

20. M. P. Allen and D. J. Tildesley, *Computer Simulation of Liquids*, (Oxford University Press, New York, 1989).

21. W. C. Swope, H. C. Andersen, P. H. Berens, and K. R. Wilson, "A computer simulation method for the calculation of equilibrium constants for the formation of physical clusters of molecules: Application to small water clusters", *Journal of Chemical Physics* 76, 1 (1982).

22. K. Nordlund, "PARCAS computer code. The main principles of the molecular dynamics algorithms are presented in [23, 24]. The adaptive timestep is used as in [26]"

23. K. Nordlund, M. Ghaly, R. S. Averback, M. Caturla, T. Diaz de la Rubia and J. Tarus, "Defect production in collision cascades in elemental semiconductors and FCC metals", *Physical Review B* 57, 7556 (1998).

24. M. Ghaly, K. Nordlund and R. S. Averback, "Molecular dynamics investigations of surface damage produces by keV self-bombardment of solids", *Phylosophical Magazine A* 79, 795, (1999).

25. C. W. Gear, *Numerical Initial Value Problems in Ordinary Differential Equations*, (Upper Saddle River, NJ, USA: Prentice Hall PTR, 1971).

26. K. Nordlund, "Molecular dynamics simulation of ion ranges in the 1–100 kev energy range", *Computational Materials Science* 3, 448 (1995).

27. H. Berendsen, J. Postma, W. van Gunsteren, A. DiNola and J. Haak, "Molecular dynamics with coupling to an external bath", *Journal of Chemical Physics* 81, 3684 (1984).

28. M. Z. Bazant, E. Kaxiras, and J. F. Justo, "Environment-dependent interatomic potential for bulk silicon", *Physical Review B* 56, 8542 (1997).

29. M. de Koning, A. Antonelli, M. Z. Bazant, E. Kaxiras and J. F. Justo, "Finite temperature molecular-dynamics study of unstable stacking fault energies in silicon", *Physical Review B* 58, 12555 (1998).

30. N. Bernstein, M. J. Aziz, and E. Kaxiras, "Atomistic simulations of solid-phase epitaxial growth in silicon", *Physical Review* 61, 6696 (2000).

31. S. M. Daw and M. I. Baskes, "Embedded-atom method: Derivation and application to impurities, surfaces, and other defects in metals", *Physical Review B* 29, 6443 (1984).

32. S. M. Daw, S. M. Foiles and M. I. Baskes, "The embedded-atom method: a review of theory and applications", *Materials Science Reports* 9, 251 (1993).

33. M. T. Robinson and I. M. Torrens, "Computer simulation of atomic-displacement cascades in solids in the binary-collision approximation", *Physical Review B* 9, 5008 (1974).

34. M. T. Robinson, "Computer simulation studies of high-energy collision cascades", *Nuclear Instruments and Methods in Physics Research Section B: Beam Interactions with Materials and Atoms* 67, 396 (1992).

35. F. G. Djurabekova, T. S. Pugacheva, F. F. Umarov and S. V. Yugay, "Computer Simulation of Ion Implantation with Visual Observation of the Implantation Profiles", International Conference on Ion Implantation Technology Proceedings. Ion Implantation Technology (2000).

36. S. Harada, S. Yokota, Y. Ishii, Y. Shizuku, M. Kanazawa and Y. Fukai, "A relation between the vacancy concentration and hydrogen concentration in the Ni–H, Co–H and Pd–H systems", *Journal of Alloys and Compounds* 404, 247 (2005).

37. Y. Fukai and H. Sugimoto, "Formation mechanism of defect metal hydrides containing superabundant vacancies", *Journal of Physics: Condensed Matter* 19, 436201 (2007).

38. A. C. Damask and G. J. Dienes, *Point Defects in Metals*, (Gordon and Breach, New York, 1963).

39. M. W. Guinan, R. N. Stuart and R. J. Borg, "Fully dynamic computer simulation of self-interstitial diffusion in tungsten", *Physical Review B* 15, 699 (1977).

40. K-D. Rasch, R. W. Siegel and H. Schultz, "Quenching and recovery investigations of vacancies in tungsten", *Philosophical Magazine A* 41, 91 (1980).

41. C. S. Becquart, C. Domain, U. Sarkar, A. DeBacker and M. Hou, "Microstructural evolution of irradiated tungsten: Ab initio parameterisation of an OKMC model", *Journal of Nuclear Materials* 403, 75 (2010).

42. T. Ahlgren, K. Heinola, N. Juslin and A. Kuronen, "Bond-order potential for point and extended defect simulations in tungsten", *Journal of Applied Physics* 107, 033516 (2010).

43. D. Nguyen-Manh, A. P. Horsfield, and S. L. Dudarev, "Self-interstitial atom defects in bcc transition metals: Group-specific trends", *Physical Review B* 73, 020101 (2006).

44. N. Juslin, P. Erhart, P. Träskelin, J. Nord, K.O.E. Henriksson, K. Nordlund, E. Salonen and K. Albe, "Analytical interatomic potential for modeling nonequilibrium processes in the W–C–H system", *Journal of Applied Physics* 98, 123520 (2005).

45. Xiao-Chun Li, Xiaolin Shu, Yi-Nan Liu, F. Gao, Guang-Hong Lu. "Modified analytical interatomic potential for a W–H system with defects", *Journal of Nuclear Materials* 408, 12 (2011).

46. P. M. Derlet, D. Nguyen-Manh and S. L. Dudarev, "Multiscale modeling of crowdion and vacancy defects in body-centered-cubic transition metals", *Physical Review B* 76, 054107 (2007).

47. K. Heinola and T. Ahlgren, "First-principles study of h on the reconstructed w(100) surface", *Physical Review B* 81, 073409 (2010).

48. I. M. Neklyudov, E. V. Sadanov, G. D. Tolstolutskaja, V. A. Ksenofontov, T. I. Mazilova and I. M. Mikhailovskij, "Interstitial atoms in tungsten: Interaction with free surface and in situ determination of formation energy", *Physical Review B* 78, 115418 (2008).

49. A. Satta, F. Willaime and S. de Gironcoli, "Vacancy self-diffusion parameters in tungsten: Finite electron-temperature LDA calculations", *Physical Review B* 57, 11184 (1998).

50. R. Frauenfelder, "Solution and diffusion of hydrogen in tungsten", *Journal of Vacuum Science and Technology* 6, 388 (1969).

51. K. Heinola, T. Ahlgren, K. Nordlund and J. Keinonen, "Hydrogen interaction with point defects in tungsten", *Physical Review B* 82, 094102, (2010).

52. C. Becquart and C. Domain, "A density functional theory assessment of the clustering behaviour of He and H in tungsten", *Journal of Nuclear Materials* 386, 109 (2009).

53. Y. Liu, Y. Zhang, G. Luo and G. Lu, "Structure, stability and diffusion of hydrogen in tungsten: A first-principles study", *Journal of Nuclear Materials*, 390, 1032 (2009).

54. S. A. Mollick, D. Ghose, P. D. Shipman and R. M. Bradley, "Anomalous patterns and nearly defect-free ripples produced by bombarding silicon and germanium with a beam of gold ions", *Applied Physics Letters* 104, 043103 (2014).

55. W. L. Chan and Eric Chason, "Sputter ripples and radiation-enhanced surface kinetics on Cu(001)", *Physical Review B* 72, 165418, (2005).

56. V. I. Shulga, "Sputtering of platinum by argon ions: A simulation study", *Nuclear Instruments and Methods in Physics Research Section B: Beam Interactions with Materials and Atoms* 174, 423 (2001).

57. S. Norris, J. Samela, L. Bukonte, M. Backman, F. Djurabekova, K. Nordlund, C. S. Madi, M. P. Brenner, and M. J. Aziz, "Molecular dynamics of single-particle impacts predicts phase diagrams for large scale pattern formation", *Nature Communications* 2, 276, (2011).